BBA - Bioenergetics 1862 (2021) 148413

Contents lists available at ScienceDirect

BBA - Bioenergetics

journal homepage: www.elsevier.com/locate/bbabio

Trehalose matrix effects on electron transfer in Mn-depleted protein-pigment complexes of Photosystem II

Mahir D. Mamedov [a], Georgy E. Milanovsky [a], Marco Malferrari [b,1], Liya A. Vitukhnovskaya [a,c], Francesco Francia [b], Alexey Yu. Semenov [a,c,*], Giovanni Venturoli [b,d,**]

[a] A.N. Belozersky Institute of Physical-Chemical Biology, Lomonosov Moscow State University, 119992 Moscow, Leninskye gory, 1, b.40, Russia
[b] Laboratory of Biochemistry and Molecular Biophysics, Department of Pharmacy and Biotechnology, FaBiT, University of Bologna, Bologna, Via Irnerio, 42, Italy
[c] N.N. Semenov Federal Research Center for Chemical Physics, Russian Academy of Sciences, Moscow, 119991, Kosygina Street, 4, b.1, Russia
[d] Consorzio Nazionale Interuniversitario per le Scienze Fisiche della Materia, CNISM, c/o Department of Physics and Astronomy "Augusto Righi", DIFA, University of Bologna, Bologna, Via Irnerio, 46, Italy

ARTICLE INFO

Keywords:
Photosystem II
Electron transfer
Trehalose
Matrix effect
Protein dynamics

ABSTRACT

The kinetics of flash-induced re-reduction of the Photosystem II (PS II) primary electron donor P_{680} was studied in solution and in trehalose glassy matrices at different relative humidity. In solution, and in the re-dissolved glass, kinetics were dominated by two fast components with lifetimes in the range of 2–7 μs, which accounted for >85% of the decay. These components were ascribed to the direct electron transfer from the redox-active tyrosine Y_Z to $P_{680}^{\bullet+}$. The minor slower components were due to charge recombination between the primary plastoquinone acceptor $Q_A^{\bullet-}$ and $P_{680}^{\bullet+}$. Incorporation of the PS II complex into the trehalose glassy matrix and its successive dehydration caused a progressive increase in the lifetime of all kinetic phases, accompanied by an increase of the amplitudes of the slower phases at the expense of the faster phases. At 63% relative humidity the fast components contribution dropped to ~50%. A further dehydration of the trehalose glass did not change the lifetimes and contribution of the kinetic components. This effect was ascribed to the decrease of conformational mobility of the protein domain between Y_Z and P_{680}, which resulted in the inhibition of $Y_Z \rightarrow P_{680}^{\bullet+}$ electron transfer in about half of the PS II population, wherein the recombination between $Q_A^{\bullet-}$ and $P_{680}^{\bullet+}$ occurred. The data indicate that PS II binds a larger number of water molecules as compared to PS I complexes. We conclude that our data disprove the "water replacement" hypothesis of trehalose matrix biopreservation.

1. Introduction

The incorporation of proteins into glassy matrices formed by the disaccharide trehalose represents a valuable approach to unravel the intimate association between internal protein motions and protein function. Due to its high glass transition temperature [1], trehalose can form solid amorphous matrices at room temperature even at high hydration levels. By reducing progressively the content of residual water within the glassy matrix, a tight dynamical coupling between the embedded protein and the increasingly stiffened matrix is established, which results in a progressive retardation of the conformational dynamics of the incorporated protein. Under extreme dehydration (corresponding to about 0.5 water molecule per trehalose molecule of the matrix), a dramatic hindering of internal protein motions can be attained (for reviews see [2–4]). This makes possible to investigate at room temperature the role of protein dynamics in specific protein catalytic events, avoiding the freezing of the protein to cryogenic temperatures to reduce internal protein motions. As an additional advantage,

Abbreviations: PS, photosystem; Chl, chlorophyll; bRC, bacterial photosynthetic reaction center; Y_Z, redox-active tyrosine-161 of D1 subunit of PS II; PQ, plastoquinone; PQH_2, plastohydroquinone; DM, *n*-dodecyl β-D-maltoside; MEM, maximum entropy method.

* Correspondence to: A.Yu. Semenov, A.N. Belozersky Institute of Physical-Chemical Biology, Lomonosov Moscow State University, 119992 Moscow, Leninskye gory, 1, b.40, Russia.

** Correspondence to: G. Venturoli, Laboratory of Biochemistry and Molecular Biophysics, Department of Pharmacy and Biotechnology, FaBiT, University of Bologna, Bologna, BO, Via Irnerio, 42, Italy.

E-mail addresses: semenov@belozersky.msu.ru (A.Yu. Semenov), giovanni.venturoli@unibo.it (G. Venturoli).

[1] Present address: Department of Chemistry "Giacomo Ciamician", University of Bologna, Bologna BO, 40126, Via Selmi, 2, Italy.

https://doi.org/10.1016/j.bbabio.2021.148413
Received 8 December 2020; Received in revised form 15 February 2021; Accepted 7 March 2021
Available online 12 March 2021

the incorporation into dehydrated trehalose glasses results in extraordinary thermal stabilization of the embedded protein; when incorporated into the trehalose solid matrix, even labile proteins can withstand high temperatures without undergoing thermal denaturation [5–8].

In a series of previous studies [9–15] we have addressed trehalose matrix effects on the electron transfer processes catalyzed by the bacterial photosynthetic reaction center (bRC) from *Rhodobacter (Rba.) sphaeroides*. We showed that the incorporation of the bRC into trehalose glassy matrices at low water content deeply affects both the forward electron transfer from the primary $Q_A^{-\bullet}$ to the secondary quinone acceptor Q_B and the kinetics of charge recombination between the primary quinone acceptor $Q_A^{\bullet -}$ and the primary electron donor ($P^{\bullet +}$). The former reaction was reversibly and *heterogeneously* inhibited [10], mimicking at room temperature the behaviour observed when hydrated bRCs are frozen in the dark at cryogenic temperatures [16], and providing evidence for a conformationally-gated electron transfer mechanisms [17]. In progressively dehydrated trehalose glasses, the kinetics of $P^{\bullet +}Q_A^{\bullet -}$ recombination became progressively faster and non-exponential [9], showing that the conformational relaxation from the dark- to the light-adapted state, which stabilizes the primary $P^{\bullet +}Q_A^{\bullet -}$ charge separated state [18], as well as the interconversion among bRC conformational substates, are completely blocked within the trehalose glass, on the time scale of charge recombination. The study of trehalose-matrix effects on long range electron transfer has been subsequently extended to the cyanobacterial photosystem I (PS I) [19,20], characterized by a much higher structural complexity, as compared to bRC. It was found essentially that, again mimicking low temperature effects [21], dehydration of the trehalose matrix caused a progressive block of the forward electron transfer from F_X^- to the terminal F_A/F_B acceptors in an increasing fraction of the PS I population, and that, under the driest condition of the trehalose matrix, also the forward electron transfer from the photoreduced phylloquinones $A_{1A}^{\bullet -}$ and $A_{1B}^{\bullet -}$ in the symmetrical branches of redox-cofactors to the iron-sulfur 4Fe4S clusters F_X, F_A and F_B was prevented in a PS I sub-population. Matrix dehydration resulted in progressively more distributed kinetics of $P_{700}^{\bullet +}F_X^{\bullet -}$ recombination, revealing, as already observed in the case of bRCs, the trapping of PS I conformational substates at room temperature. It is noteworthy that parallel high-resolution EPR investigations, performed on both bRCs [12] and PS I complexes [19], indicated that the embedding into dehydrated trehalose glass did not affect the distance and relative orientation of cofactors involved in electron transfer. It can therefore be concluded that embedded proteins are softly confined by trehalose glasses [4], and that the observed trehalose matrix effects on electron transfer processes can be essentially ascribed to inhibition of the protein conformational dynamics.

Encouraged by the results summarized above, we have exploited in the present work the use of trehalose glasses to examine matrix effects on electron-transfer reactions catalyzed by the other photosystem, Photosystem II (PS II), of oxygenic photosynthesis, for which low-temperature studies [22,23] suggest a role of protein internal dynamics in electron transfer.

PS II enzymatically functions as light-driven water-plastoquinone oxidoreductase. PS II core complexes (~350 kDa for monomer), containing the minimal set of proteins required to oxidize water in vitro [24,25], are highly conserved between cyanobacteria, plants and algae [26,27]. The redox-active cofactors, which reside in the D1D2 reaction center (RC) and carry out light-induced charge separation, include four chlorophyll (Chl) *a* molecules and two pheophytin *a* molecules. The primary (Q_A) and secondary (Q_B) plastoquinone molecules are reduced in sequence on the acceptor side of the RC [28,29]. The water-oxidizing complex (WOC), located at the donor side of PS II, consists of an inorganic Mn_4CaO_5 metal cluster bound to the surrounding protein matrix [25].

The extrinsic proteins of PS II (named PsbO, PsbU, and PsbV in the case of cyanobacteria; PsbO, PsbP, PsbQ, and PsbR in higher plants) shield the catalytic Mn_4CaO_5 cluster from exogenous reductants (reviewed in [30,31]). The two integral membrane protein subunits CP43 and CP47, attached to both sides of the RC, contain Chl *a* and β-carotene molecules and act as internal antenna complexes [25,32]. These antenna proteins are in close contact with the membrane-extrinsic subunits [32].

Following photon absorption electron transfers from the primary electron donor, P_{680}, to the primary quinone acceptor Q_A resulting in the formation of an ion-radical pair ($P_{680}^{\bullet +}Q_A^{\bullet -}$) within ~250 ps. Under physiological conditions, the reduction of $P_{680}^{\bullet +}$ occurs because of transfer of an electron from the redox-active tyrosine-161 of D1 subunit of PS II (denoted in the following as Y_Z) in the nanosecond (20–250 ns) time range. In doing so, Y_Z radical cation is stabilized by losing a proton to the neighboring D1-His190 in a reversible fashion, forming a neutral tyrosine radical ($Y_Z^{\bullet}$) [33–37]. Two different chemical reactions, namely reduction of plastoquinone (PQ) to plastohydroquinone (PQH_2) in the Q_B-site (after two turnovers of PS II) and oxidation of water to molecular oxygen (after four turnovers of PS II) (see [38–41] for details) take place on the acceptor and donor sides, respectively.

The water-splitting process involves the dark stable S_1, and S_2, S_3 and S_4 intermediate states of the WOC of PS II [37,41]. A complete enzyme turnover takes ~10 ms [40] and is limited by the slowest reactions on the quinone reduction side of PS II [42]. Outlined above reactions are spatially separated and occur on different sides of the RC in the thylakoid membrane (see Fig. 1). It should be stressed that within the PS II RC complex the WOC is highly susceptible to photo-oxidative damage and other stress conditions (see [43] and Refs therein).

Removal of the Mn_4CaO_5 cluster from the intact PS II core complex results in significant retardation of the $Y_Z \rightarrow P_{680}^{\bullet +}$ electron transfer. The oxidation of tyrosine Y_Z in Mn-depleted complexes exhibits half-lives of

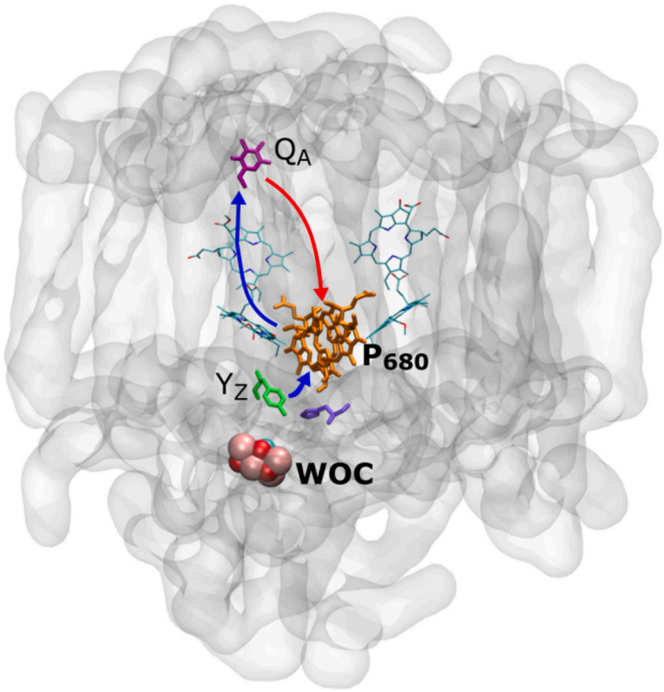

Fig. 1. Arrangement of electron transfer cofactors in Photosystem II, based on the cryo-EM structure of the complex from spinach (PDB ID: 3JCU). The primary electron donor P_{680} (orange) and quinone acceptor Q_A (magenta) are represented by thick wireframe models, accessory chlorophylls Chl_{D1} and Chl_{D2} and pheophytins *a* $Pheo_{D1}$ and $Pheo_{D2}$ by thin wireframes; the metal cluster of the water-oxidizing complex is shown as Van der Waals spheres. Blue arrows indicate forward electron transfer reactions from P_{680} to Q_A and from tyrosine Y_Z to the photoxidized P_{680}; the red arrow indicates charge recombination between $P_{680}^{\bullet +}$ and $Q_A^{\bullet -}$. D1-His190 residue, stabilizing the cation on Y_Z, is shown in violet.

~30 μs at pH 4, ~5 μs at pH 6.5 and ~180 ns above pH 8.5 [23,44–46] and this reaction shows a kinetic H/D isotope exchange effect [35,47,48]. It is believed that the phenolic side chain of Y_Z is most likely protonated in the reduced state and deprotonated in the oxidized state. The transferred proton is thought to be accepted by D1-His190, which forms a hydrogen bond to Y_Z [35,48]. The slowing of the rate of charge transfer in Mn-depleted samples can be due to the alteration of the local dielectric permittivity of the surrounding protein [49], to rearrangement of the hydrogen-bonding network, as well as to perturbation of pK-values [23,35].

Based on the measurements of the fluorescence of PS II membrane fragments, it was long believed that when the Mn_4CaO_5 cluster is impaired, $E_m(Q_A^-/Q_A)$ is significantly upshifted (100 mV) [50–52]. It is also known that upon inactivation of the Mn-cluster, the values of $E_m(Q_B^-/Q_B)$ and $E_m(Fe^{2+}/Fe^{3+})$ change slightly [53,54]. It was thus proposed that the resulting large ΔG decrease of $Q_A^- \rightarrow Q_B$ electron transfer shifts the electron transfer equilibrium from Q_B^- to Q_A in a fraction of PS II, facilitating direct charge recombination between $Q_A^{\bullet -}$ and $P_{680}^{\bullet +}$ [54]. However, the mechanism of this long-distance interaction between the Mn_4CaO_5 cluster and Q_A (~40 Å) in PS II remains unresolved. In addition, the determination of the structure of PS II complexes showed that removal of the Mn-cluster did not result in any discernible movement of subunits or domains either on the donor or on the acceptor sides of PS II [55]. Finally, reinvestigation the $E_m(Q_A^-/Q_A)$ using FTIR spectroelectrochemistry, which can directly monitor the redox state of Q_A showed that the $E_m(Q_A^-/Q_A)$ value is not affected by depletion of the Mn-cluster [56]. The authors thus concluded that the Mn_4CaO_5 cluster does not directly regulate the redox potentials of the iron-quinone electron acceptors, although the effect of the extrinsic proteins is still a question to be answered.

Normally recombination of $P_{680}^{\bullet +}Q_A^{\bullet -}$ is prevented because $P_{680}^{\bullet +}$ oxidizes Y_Z with polyphasic kinetics in the 10^{-7} to 10^{-5} s time range [47]. The kinetics of PS II charge recombination is well characterized when forward electron transfer from Y_Z is blocked, as a result of inactivation of the WOC and pre-illumination of PS II samples to keep Y_Z oxidized [57]. A characteristic time for $P_{680}^{\bullet +}Q_A^{\bullet -}$ recombination of near 170 μs is then observed in plant PS II [44,57–59]. In mutant cyanobacterial Y_Z-less PS II complexes, the kinetics of $P_{680}^{\bullet +}Q_A^{\bullet -}$ appear to be slower by almost one order of magnitude [60–62].

The effect of dehydration has been studied in films formed by PS II membrane fragments under defined relative humidity [63], focusing on the photoaccumulation of $Q_A^{\bullet -}$ and redox reactions on the donor side induced by continuous illumination. It was concluded that hydration does not affect light-induced charge separation, but severely impairs the reduction of Q_B by $Q_A^{\bullet -}$ and the reactions of the water splitting complex.

In the present work, we have examined trehalose matrix effects on the kinetics of reduction of $P_{680}^{\bullet +}$ photoxidized by a laser pulse in Mn-depleted PS II complexes, as a function of the residual water content of the trehalose glass. We have found that, upon reducing progressively the hydration of the matrix, the electron transfer from Y_Z is blocked in an increasing fraction of the PS II population, allowing kinetic analysis of $P_{680}^{\bullet +}Q_A^{\bullet -}$ recombination, which accounts for about 50% of $P_{680}^{\bullet +}$ re-reduction at sufficiently low hydration values.

2. Materials and methods

2.1. Isolation of PS II complexes

Highly active PS II core complexes were prepared from market spinach according to Haag and coworkers [64] by treatment of the membrane fragments with *n*-dodecyl β-D-maltoside (DM) (10:1, detergent/chlorophyll) for 1 h followed by sucrose density centrifugation (20–40%) for 16 h at 145000*g*. After preparation, samples were frozen in liquid nitrogen and stored at −70 °C in 50 mM MES (2-morpholinoethanesulfonic acid, pH 6.5), 10 mM NaCl, 20 mM $CaCl_2$, 0.03% (w/v) DM (buffer A) in Eppendorf vials at a Chl concentration of 2–3 mg/mL. The Chl *a*/Chl *b* ratio was 6. A quantitative determination of the Chl content of the PS II core complex revealed about 50 Chl *a* molecules/complex. The rate of O_2 evolution under continuous illumination with saturating white light at 23 °C was about 1600–1700 μmol mg Chl^{-1} h^{-1}. Chl concentration was determined in 80% acetone-water mixture according to [65].

Mn-depleted PS II particles were prepared by incubation of PS II core complexes (0.5 mg Chl mL^{-1}) in an equal volume of buffer containing 0.8 M Tris–HCl (pH 8.3) and 2 mM EDTA under dim light for 30 min at 23 °C. The PS II suspension was then washed three times with 25 mM MES-NaOH (pH 6.5) and finally resuspended in buffer A.

2.2. Sample preparation and determination of residual water content in trehalose-PS II glassy matrices

Trehalose-PS II glassy matrices were prepared following essentially the procedure previously used to incorporate into trehalose glasses bRCs [14] and PS I [19]. Trehalose (>99% purity) was used as supplied by Sigma-Aldrich. To obtain trehalose-PS II glasses characterized by a trehalose/PS II molar ratio equal to 10^4, a 50 μL drop, containing typically PS II corresponding to 1.15 mg Chl/mL in 50 mM MES, pH 6.5, 0.03% (w/v) DM, 250 mM trehalose, 5 mM NaCl, 10 mM $CaCl_2$, was deposited on a CaF_2 optical window and dried at room temperature by gently flowing N_2 gas on its surface. Amorphous matrices characterized by different trehalose/PS II molar ratio were prepared by keeping constant the PS II concentration and adjusting appropriately the trehalose concentration.

The hydration of the trehalose-PS II glassy matrix was controlled by the isopiestic method described in detail in [66,67]. The optical window, on which the glass was formed, was inserted in a gas-tight holder and equilibrated with different saturated salt solutions placed at the bottom of the holder to provide defined values of relative humidity *r*. We used the following saturated salt solutions to obtain, at room temperature, the different *r* values (indicated in brackets): NaCl (74%), NH_4NO_3 (63%), $Mg(NO_3)_2$ (53%), K_2CO_3 (43%), $MgCl_2$ (33%), LiCl (11%), $NaOH{\cdot}H_2O$ (6%) [68].

The content of residual water in the trehalose-PS II matrices was determined from the area under the NIR ($\nu_2 + \nu_3$) combination band of water at 5155 cm^{-1} as described in [19], using an absorptivity value of 102 absorbance unit nm M^{-1} cm^{-1}. As an internal standard, we used the NIR trehalose band at 4760 cm^{-1} which is ascribed to combinations of C-O-H bending and OH stretching modes [69,70]. For this trehalose band an absorptivity value of (3.3 ± 0.3) 10^2 nm M^{-1} cm^{-1} has been previously determined [19]. NIR spectra were acquired by using a Jasco Fourier-transform 6100 spectrometer equipped with a DLATGS detector as described in [66].

2.3. Near-infrared time-resolved optical spectroscopy and data analysis

The kinetics of re-reduction of the primary electron donor $P_{680}^{\bullet +}$ photoxidized by a flash of light were studied by recording the transient absorption changes at 820 nm [71], using an optical bench of local design. The monitoring beam (25 mW output power), provided by a L808P200 laser diode (Thorlabs, Newton, NJ, USA), was collimated by a single lens placed between the laser diode and the sample holder. This allowed to position the detector at a large (>50 cm) distance from the sample, thus reducing the solid angle of fluorescence collection from the sample by the detector. In fact, a limit in the measurement of fast absorbance transients at 820 nm comes from the flash-induced fluorescence of the sample. The set up described above significantly decreased fluorescence artifacts, allowing the measurements of absorption change after a few hundreds of nanoseconds following the laser flash. In order to determine precisely the residual artifact, control measurements were performed in which the detector signal was recorded after a laser pulse in the presence of PS II samples with the 820 nm measuring beam switched off. The signal (see Fig. S2 of Supplementary Material)

completely vanishes 350 ns after the laser pulse. In view of this, when examining absorbance changes at 820 nm, the initial, rapidly decaying transient corresponding to the duration of the artifact was omitted. The NIR radiation was detected by a reverse-biased PIN silicon photodiode, matched to a Thorlabs, PDA36A amplifier with 17 MHz bandwidth. The photodiode was shielded from scattered excitation light by a long-pass glass filter (780 nm cut-on wavelength) and by a 10^{-4} blocking, 10 nm bandwidth interference filter centered at 820 nm.

Pulsed photoexcitation of PS II was accomplished by a sulforhodamine B dye cavity (Pulsed Dye Laser RDP-1, Radiant Dyes Laser GmbH, Wermelskirchen, Germany), emitting at 587 nm, pumped by a frequency doubled Q-switched Nd:YAG laser (Handy 710, Quanta System, Milano, Italy) delivering 7 ns width pulses at 532 nm. The energy of photoexcitation pulses at 587 nm, measured on the sample, was 8 mJ. The plane of the optical window carrying the trehalose-PS II matrices formed a 45° angle with both the measuring and excitation laser beams in order to minimize reflection of the excitation pulse towards the detector.

Transient signals from the detector amplifier were digitized by a LeCroy 9410 digital oscilloscope interfaced to an Olivetti M290 personal computer. In order to capture with the appropriate time resolution the entire decay kinetics, covering four orders of magnitude in time, generally three kinetic traces were collected in sequential, separate measurements, by using sweeps of increasing duration and sampling time (100 μs sweep, sampled every 0.01 μs; 2.5 ms sweep, sampled every 0.25 μs; 10 ms sweep, sampled every 1 μs). In the overlapping time intervals an excellent agreement between the traces at different time resolution was found. The final trace, which was used in the kinetic analysis, was obtained by merging the kinetic traces acquired on the different time scale, avoiding overlapping and keeping the maximal resolution available. Typically 200 signals were averaged at 1 Hz pulse repetition rate.

Measurements on PS II solution were performed on a 120 μL volume in a quartz cuvette with 10 mm optical path length, containing PS II corresponding typically to 200 μM Chl in 50 mM MES, pH 6.5, and 0.03% (w/v) DM.

The numerical analysis of multiphasic kinetic signals has been performed by using different software programs, i.e. the CONTIN [72] program, The MemExp 4.0 package [73,74], the IGOR Pro software (Wavemetrics, Lake Oswego, OR, USA), and locally developed QBasic routines. Confidence intervals of the fitting parameters have been evaluated numerically through exhaustive search methods [75,76] as described in detail in [13].

Molecular graphics and analyses of water bound to the PS II complex have been performed with the program UCSF Chimera [77].

3. Results

3.1. The hydration of trehalose-PS II glassy matrices under controlled relative humidity

When studying matrix effects in disaccharide-protein glasses, the control of the hydration level of the glassy matrix and the determination of the residual water content are of utmost importance. The structural and dynamical properties of trehalose amorphous matrices have been shown in fact to be critically determined by their hydration level [78], which additionally governs the dynamical coupling between the trehalose matrix and the embedded protein, strongly affecting the extent of protein conformational immobilization within the glass [2,9,79]. We have therefore primarily studied water sorption by trehalose-PS II glassy matrices, equilibrated at different values of relative humidity. As detailed under Materials and methods, the hydration level of the trehalose-PS II matrices has been controlled over a wide range by exposing the amorphous samples to atmospheres of defined relative humidity provided by different saturated salt solutions. The content of residual water in the protein disaccharide glass has been determined by FTIR spectroscopy from the area of the ($\upsilon_2 + \upsilon_3$) combination band of water centered at 5155 cm^{-1}. NIR spectra recorded in a trehalose glass incorporating Mn-depleted PS II complexes, equilibrated at different values of relative humidity, are shown in Fig. S1 of Supplementary Material. Spectroscopic measurements were performed directly on the glassy matrix exposed to the saturated atmosphere inside the sample holder. This allowed monitoring hydration changes during the incubation at any defined relative humidity, checking the attainment of steady water contents, i.e. of equilibrium.

The results of a series of such measurements are collected in Table 1, which shows the water content, expressed as water/trehalose molar ratio, measured in trehalose glasses embedding intact or Mn-depleted PS II complexes, equilibrated at relative humidity r ranging between 53% and 6%. Consistent results have been obtained following dehydration and re-hydration sequences, confirming the attainment of equilibrium water sorption values and the absence of hysteresis effects. For the sake of comparison, Table 1 includes data obtained in a previous study performed by using a similar approach in trehalose-PS I glasses [19]. Upon decreasing the relative humidity from 53% to 33%, the residual water content of trehalose glasses incorporating both intact or Mn-depleted PS II complexes decreases progressively, but equilibration at lower values of relative humidity, even under extremely drying conditions ($r = 6\%$), does not further affect, within the experimental error, the hydration level of the matrix, which remains steadily around 1.1 and 1.3 water per trehalose molecule for the matrices containing Mn-depleted and intact PS II complexes, respectively. This behaviour is at variance with what observed in trehalose-PS I glassy matrices, where the content of residual water decreases monotonically upon decreasing the relative humidity from $r = 53$ to $r = 11\%$ [19]. Additionally, the hydration of the trehalose-PS I matrices is systematically lower than that of trehalose-PS II glasses, particularly in extensively dried matrices, reaching contents of residual water per trehalose molecule as low as ~0.5 at $r = 11\%$ [19]. This value coincides, within the experimental uncertainty, with that determined in a binary trehalose-water glassy matrix [78], in the absence of any protein complex. The values of water/trehalose molar ratios determined in trehalose-protein matrices result from the overall hydration of the system, and therefore include in principle water molecules adsorbed to the bulk trehalose matrix as well as water molecules bound to the embedded protein, belonging to the residual protein hydration shell (see Discussion). The former contribution (water bound to bulk trehalose molecules) is expected to prevail in the matrices

Table 1
Residual water content of trehalose glasses embedding Mn-depleted PS II, intact PS II, and PS I complexes, equilibrated at different values of relative humidity, r (see Section 3.1 for details). Where indicated, standard errors have been calculated from measurements on at least 5 different matrices equilibrated at the indicated r values.

Relative humidity, r (%)	6	11	23	33	43	53
H_2O/trehalose molar ratio Mn-depleted PS II-trehalose glass[a]	1.05 ± 0.05	1.16 ± 0.07	1.04 ± 0.02	1.09 ± 0.03	1.72 ± 0.08	2.65 ± 0.02
H_2O/trehalose molar ratio Intact PS II-trehalose glass[b]	1.33 ± 0.03	1.31 ± 0.01	1.31 ± 0.02	1.33 ± 0.02	1.57 ± 0.05	2.73 ± 0.05
H_2O/trehalose molar ratio PS I-trehalose glass[c]	–	0.45	–	0.86	1.45	2.22

[a] Matrix characterized by a trehalose/PS II monomer molar ratio equal to $4.8 \cdot 10^4$.
[b] Matrix characterized by a trehalose/PS II monomer molar ratio equal to $3.5 \cdot 10^4$.
[c] Matrix characterized by a trehalose/PS I monomer molar ratio equal to $6.7 \cdot 10^4$. Data are from reference [19].

examined in Table 1, which are characterized by a very high trehalose/protein molar ratio (between 10^4 and 10^5). The coincidence of the hydration detected at $r = 11\%$ in trehalose-PS I glasses and in glasses formed only by trehalose, at the same relative humidity, suggests that the number of water molecules bound to the PS I complexes is sufficiently low to be negligible in comparison with the total number of water molecules bound to the bulk trehalose matrix embedding the protein complex, at least at the high trehalose/PS I molar ratio characterizing the matrix ($\sim 7 \cdot 10^4$). Quite remarkably this conclusion does not hold in the case of trehalose-PS II glasses, which, although being characterized by a trehalose/PS II molar ratio of the same order of magnitude ($\sim 5 \cdot 10^4$) of trehalose-PS I matrices, exhibit at $r = 11\%$ a value of water per trehalose molecule more than two times higher. This finding indicates that the hydration shell of PS II complexes includes a number of water molecules much higher than PS I, and that such a large protein hydration is retained within the trehalose matrix at low ($r = 11\%$) relative humidity. Interestingly, at variance with what observed in trehalose-PS I glasses, the equilibrium hydration of the trehalose-PS II glassy matrices remains constant upon decreasing the relative humidity from 33% to 6%, suggesting that such a higher hydration results from the contribution of a large pool of water molecules, tightly bound to the PS II complex, which are not removed even under extremely drying conditions ($r = 6\%$).

The much larger amount of water bound to the PS II complex suggested by the results of Table 1, as compared to PS I, is consistent with the much larger number of bound water molecules identified in the crystallographic structure of the former complex (see Discussion).

3.2. *The effect of dehydration on the re-reduction kinetics of $P_{680}^{\bullet+}$ photoxidized by a light pulse in trehalose-PS II glassy matrices*

Fig. 2 shows the kinetics of $P_{680}^{\bullet+}$ decay after a 7 ns width laser pulse, as measured at room temperature by the optical absorption change at 820 nm, in solution (50 mM MES, pH 6.5, 0.03% (w/v) DM) and in a trehalose-PS II glassy matrix, characterized by a trehalose/PS II molar ratio of 10^4. Original, not normalized kinetic traces are shown in Fig. S3 of Supplementary Material. Following vitrification under nitrogen flow, the trehalose-PS II amorphous matrix was dehydrated by equilibration at a relative humidity $r = 11\%$, in the presence of a saturated LiCl solution, and subsequently rehydrated by incubation with the appropriate saturated salt solution, yielding the desired increasing relative humidity values: $r = 33\%$, $r = 43\%$, $r = 63\%$, and $r = 74\%$. At $r > 74\%$ the glassy matrix melted. Kinetics were measured at the indicated r values or during incubation, before attainment of equilibrium. At the different hydration tested, immediately after the acquisition of the kinetics, the water content of the glassy matrix was determined by FTIR, as described in Materials and methods. Two representative kinetics, measured in a very wet and extensively dried matrix, equilibrated at $r = 74\%$ and $r = 11\%$, respectively, are represented in Fig. 2. Both in solution and in the glassy matrix, multiphasic kinetics are observed, spanning more than three orders of magnitude in time. Incorporation of the PS II complex into the trehalose glass and dehydration at $r = 11\%$ results in a drastic overall slowdown of $P_{680}^{\bullet+}$ decay as compared to solution, leading to the increase of the overall half-life of the kinetics by more than one order-of-magnitude. Upon humidification of the glassy matrix (equilibrated at $r = 74\%$) the overall kinetics become faster, but are still strongly retarded as compared to those observed in solution.

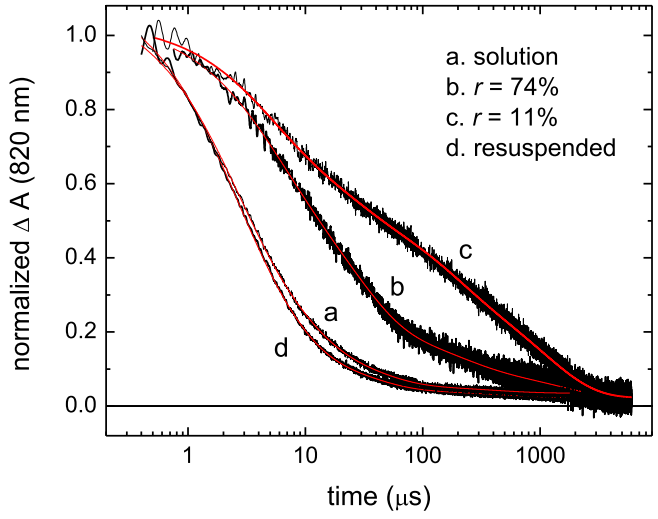

Fig. 2. Decay kinetics of $P_{680}^{\bullet+}$ following photo-oxidation by a laser pulse, as measured by NIR absorption spectroscopy at 820 nm. Kinetics recorded in solution (a) and in a trehalose-PS II glassy matrix equilibrated at two values of relative humidity, $r = 74\%$ (b) and $r = 11\%$ (c) are shown. Following dehydration at $r = 11\%$ the glass was re-dissolved and kinetics measured in the liquid re-suspended complex (*d*). Red lines represent best fitting obtained by using the program MemExp. Residuals of the fit are shown in Fig. S3 of Supplementary Material for the original, not normalized traces. See Section 3.2 for additional details.

The matrix effects described above are fully reversible, as shown by the trace acquired after re-dissolving the glass, which exhibits kinetics quite similar to those recorded in a fresh PS II solution.

The analysis of multiphasic kinetic signals, like those shown in Fig. 2, in terms of exponential processes poses often non-trivial problems. Kinetics can generally be interpreted as a sum of discrete exponential components, and the amplitude and lifetime for each kinetic phase is commonly determined by nonlinear least squares algorithms. Conventional nonlinear least squares procedures require, however, that the number of exponentials is specified a priori in the model. In addition, as the number of exponential phases increases, the search for optimal parameters can become ambiguous, depending on the initial values assigned, due to the existence of multiple chi-square minima. Alternatively, kinetics can be interpreted as reflecting continuous lifetime distributions [80], which can be in principle obtained from the kinetics using regularization methods, like the Tikhonov-Phillips method [81], implemented in the program CONTIN [72], and the maximum entropy method (MEM) [82]. In a first approach, we have fitted each kinetic signal of $P_{680}^{\bullet+}$ decay to the sum of a variable number of discrete exponentials by using locally developed least-squares minimization routines, based on the Levenberg-Marquardt algorithm [83], as well as the IGOR Pro software (Wavemetrics, Lake Oswego, OR, USA). In parallel, kinetics have been fitted to quasi-continuous lifetime distributions by using the CONTIN program [72]. Following this explorative analysis, in order to choose among the different descriptions of the kinetics (sum of three or four exponential decays or continuous lifetime distributions including a number of resolvable components varying between three and five) we have adopted the MemExp software package [73,74], which combines the MEM and non-linear least squares fitting to analyze kinetics in terms of both continuously distributed and discrete lifetimes. MemExp offers distinctive advantages: (a) it makes no a priori assumption on the number of discrete exponential phases, but adds exponential components one at a time and initializes fitting parameters based on the quasi-continuous distribution yielded by the MEM; (b) it selects an optimal distributed and discrete description of the kinetics; (c) it helps in choosing between these two alternatives by providing, besides the chi-square value of the fit, the correlation length of the residuals and the number of sign changes among residuals throughout the temporal range of the data. In Supplementary Material we provide detailed information on the different simulation approaches employed, i.e.:

(1) the kinetic parameters obtained by fitting kinetics to the sum of 3 exponential decays (Table S1),
(2) the comparison between the reduced chi-square corresponding to the best fit of the kinetics to the sum of 3 or 4 exponential decays (Table S2),

(3) the continuous distributions obtained by using the MemExp program (Fig. S4),
(4) the comparison between correlation length of the residual and number of sign changes among residuals corresponding to description of the kinetics by continuous lifetime distributions or by the sum of discrete exponential decays (Table S3).

Based on these parameters, we have concluded that the use of quasi-continuous lifetime distributions does not improve the description of the whole set of kinetic data, and that the sum of 4 discrete exponential components is the optimal choice to account for the kinetics recorded both in solution and in the glassy matrices at different relative humidity.

The results of the analysis described above are summarized in Fig. 3, which shows the lifetime (panel A) and amplitude (B) of each kinetic phase as a function of the content of residual water within the trehalose-PS II glassy matrix. Best fitting lifetimes and amplitudes are also

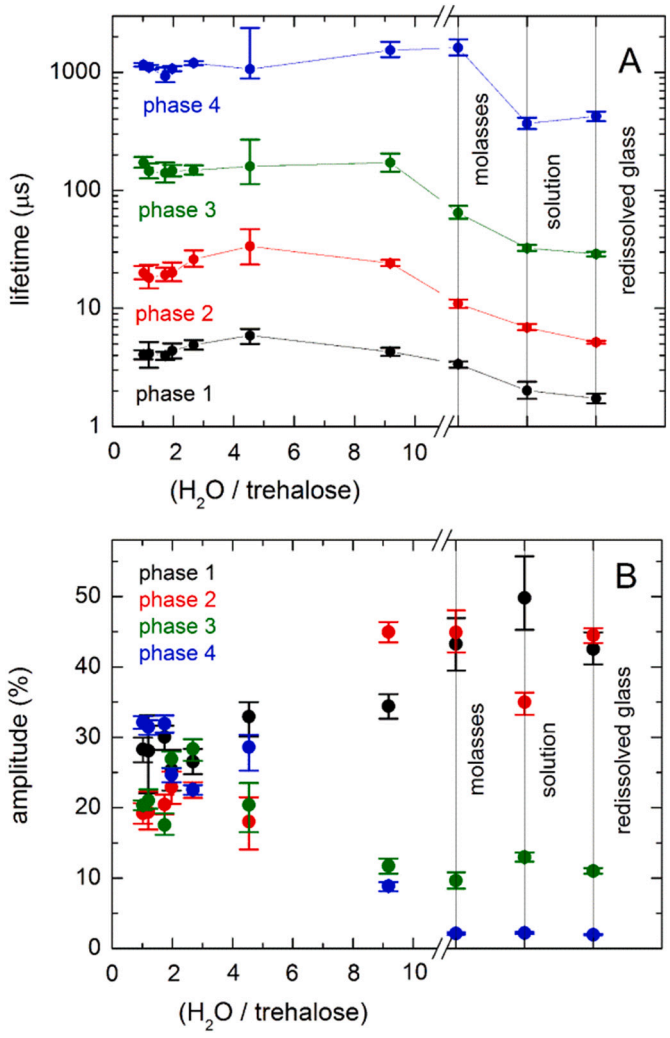

Fig. 3. Kinetic analysis of $P_{680}^{\bullet+}$ re-reduction following a laser flash as a function of the residual water content of trehalose-PS II glassy matrices. Kinetics have been fitted to the sum of discrete exponential decays by using the MemExp program. The lifetimes and the amplitudes of each of the 4 kinetic phases required to describe the kinetics are shown in panels A and B respectively. The kinetic parameters obtained by analyzing the kinetic traces recorded in solution, in a molasses at 1.12 M trehalose, and in a re-suspended trehalose-PS II glassy matrix previously equilibrated at a relative humidity $r = 11\%$ are also plotted. Vertical bars indicate confidence intervals of the fit within two standard deviations, evaluated numerically as described under Materials and methods. See Section 3.2 for further details.

reported for the kinetics measured in solution (50 mM MES, pH 6.5, 0.03% (w/v) DM) in the absence of trehalose and in the presence of a high (1.12 M) trehalose concentration. The latter solution is hereinafter referred to as "trehalose molasses". Numerical values of the best fitting kinetic parameters are given in Table 2. In solution, and in the re-dissolved glass, kinetics are dominated by the two fastest components (phase 1 and 2), characterized by lifetimes of about 2 µs and 6 µs, respectively, each kinetic phase accounting for about 40–50% of the total signal amplitude. The two residual components (phase 3 and 4) exhibit well separated lifetimes (~30 µs and ~400 µs respectively); the relative contribution of phase 4 is about 2% of the overall signal.

Addition of trehalose at high concentration (molasses) leads to a significant increase in the lifetime of all four kinetic phases, without substantially affecting their relative amplitudes. Incorporation of the PS II complex into a trehalose glass and its dehydration causes an additional progressive increase in the lifetime of the kinetic phases (except for phase 4), accompanied by a decrease of the amplitudes of the two fastest phases, compensated by an increase of the contribution of the slower phases 3 and 4. This effect is already observable in a very wet amorphous matrix, characterized by an overall water content corresponding to about 9 water molecules per trehalose molecule. Under these conditions the lifetime of phase 1 and 2 increases by a factor of ~2 and ~4, respectively, as compared to the corresponding lifetimes measured in solution; an even larger slowing (by a factor of 5 and 4 respectively) is found for phase 3 and 4. Correspondingly, the relative amplitude of the slowest phase 4 increases at the expense of phase 1. Upon decreasing the residual water content of the matrix by a factor of two, or larger, does not affect significantly the lifetimes of the kinetic components. At variance, when the H_2O/trehalose molar ratio is decreased from ~9 to ~4, the relative amplitude of phase 1 and 2 drop to about 30% and 20% respectively, while phase 3 and 4 increase to about 20% and 30% respectively. A further dehydration of the trehalose glass, down to 1 water per trehalose molecule, leads to relative amplitudes which do not appear to vary significantly, when considering the confidence intervals of the best fitting parameters.

Previous studies performed in solution on Mn-depleted PS II complexes indicate that electron transfer from Y_Z to $P_{680}^{\bullet+}$ photoxidized by a light pulse occurs on the µs time range. Lifetimes of ~10 µs and ~7.5 µs have been reported for the decay of $P_{680}^{\bullet+}$ after a laser pulse, as measured at 820 nm in Tris pretreated chloroplasts at pH 6 and 7, respectively [44]; in Tris-treated PS II particles from *Synechococcus* sp. a half-life of 4 µs has been evaluated from the kinetics of $P_{680}^{\bullet+}$ decay measured at 824 nm at pH 6.5 [45]. In a more recent work [84] multiphasic flash-induced absorption transients at 827 nm have been observed in inactive (Mn-depleted) PS II core particles from pea seedlings, and fitted to the sum of three exponential decays. At pH 6.5, the two fastest phases, characterized by comparable amplitudes, together accounting for more than 80% of the total signal amplitude, and exhibiting lifetimes around 1.5 µs and between 10 and 20 µs, have been attributed to Y_Z oxidation by $P_{680}^{\bullet+}$. The third slower component, with a half-decay time of approximately 450 µs has been shown to reflect the recombination of the charge pair $P_{680}^{\bullet+}$ $Q_A^{\bullet-}$. Based on the results summarized above, we ascribe phase 1 and 2 of our $P_{680}^{\bullet+}$ decay kinetics to electron transfer from Y_Z to $P_{680}^{\bullet+}$. The lifetimes and relative amplitudes of the two kinetic phases observed by us in liquid samples are in good agreement with the kinetic parameters of the two fastest phases reported by Junge and coworkers [84]. This study provides evidence that the slower of the two kinetic phases attributed to Y_Z oxidation reflects electron transfer rate limited by the transfer of a proton, and that the redistribution between the PS II population undergoing a fast (not limited by proton transfer) or slower (limited by proton transfer) Y_Z oxidation is governed by a protonation equilibrium with an apparent pK of ~7.0.

We interpret phase 3 and 4 of $P_{680}^{\bullet+}$ decays detected in liquid and glassy samples as reflecting charge recombination of $P_{680}^{\bullet+}$ $Q_A^{\bullet-}$. In the PS II solution and redissolved trehalose-PS II glass the lifetime of phase 4

Table 2
Kinetic parameters obtained by fitting kinetics of $P_{680}^{\bullet+}$ re-reduction to the sum of discrete exponential decays by using the program MemExp. Calculated confidence intervals within 2 standard deviations are given in brackets (see Materials and methods for details).

H_2O/trehalose molar ratio		Kinetic phase			
		1	2	3	4
1.0	τ (μs)	4.1 (3.7, 4.4)	20.0 (17.6, 22.9)	172 (155, 192)	1157 (1118, 1199)
	A (%)	28.3 (26.5, 29.9)	19.2 (17.3, 20.6)	20.4 (19.6, 21.0)	32.1 (31.2, 33.0)
1.2	τ (μs)	4.1 (3.1, 5.2)	18.2 (14.8, 23.4)	146 (126, 170)	1104 (1063, 1154)
	A (%)	28.1 (22.0, 33.1)	19.4 (16.9, 22.3)	21.0 (19.9, 22.6)	31.5 (30.4, 32.4)
1.7	τ (μs)	4.1 (3.7, 4.3)	19.3 (17.0, 22.1)	140 (116, 172)	928 (826, 1097)
	A (%)	30.0 (28.2, 31.6)	20.5 (19.0, 21.9)	17.6 (16.2, 19.2)	31.9 (30.7, 33.1)
2.0	τ (μs)	4.4 (3.8, 5.1)	20.1 (16.9, 24.5)	146 (132, 164)	1072 (1023, 1129)
	A (%)	25.4 (22.4, 28.2)	22.9 (20.6, 25.1)	26.9 (25.7, 28.0)	24.8 (23.6, 25.6)
2.7	τ (μs)	4.9 (4.5, 5.4)	26.1 (22.6, 31.0)	148 (136, 163)	1198 (1151, 1246)
	A (%)	26.5 (24.8, 28.3)	22.5 (21.4, 23.6)	28.4 (26.7, 29.7)	22.6 (21.8, 23.2)
4.5	τ (μs)	5.9 (5.0, 6.7)	33.6 (23.5, 46.9)	160 (113, 270)	1065 (889, 2378)
	A (%)	32.9 (30.1, 35.0)	18.0 (14.1, 21.5)	20.4 (16.5, 23.5)	28.7 (25.2, 30.4)
9.2	τ (μs)	4.3 (3.9, 4.6)	24.2 (22.8, 25.8)	172 (144, 205)	1542 (1347, 1812)
	A (%)	34.4 (32.6, 36.1)	45.0 (43.5, 46.4)	11.7 (10.6, 12.8)	8.9 (8.1, 9.4)
1.12 M trehalose molasses	τ (μs)	3.4 (3.1, 3.6)	11.0 (10.1, 11.9)	64.6 (57.3, 74.0)	1617 (1388, 1901)
	A (%)	43.3 (39.5, 46.9)	45.0 (42.1, 48.0)	9.6 (8.5, 12.3)	2.1 (1.9, 2.3)
Solution	τ (μs)	2.0 (1.7, 2.4)	6.9 (6.5, 7.3)	32.4 (30.7, 34.5)	369 (330, 413)
	A (%)	49.8 (45.3, 55.7)	35.0 (33.2, 36.3)	13.0 (12.3, 13.6)	2.2 (2.0, 2.4)
Resuspended glass	τ (μs)	1.7 (1.5, 1.9)	5.2 (5.0, 5.3)	28.9 (27.6, 30.2)	424 (385, 466)
	A (%)	42.5 (40.3, 44.9)	44.5 (43.4, 45.5)	11.1 (10.6, 11.4)	1.9 (1.8, 2.0)

(~400 μs) is close to that of the slowest kinetic component detected by Junge and coworkers [84] in Mn-depleted PS II core particles, which has been ascribed to charge recombination of $P_{680}^{\bullet+}$ $Q_A^{\bullet-}$. This attribution has been tested in the same study by monitoring directly the reoxidation kinetics of $Q_A^{\bullet-}$ at 320 nm. The reported relative amplitude of the slowest kinetic component of $P_{680}^{\bullet+}$ decay matches the overall contribution of phase 3 and 4 observed by us in liquid samples. Interestingly, the UV transients of the quinone anion after a laser pulse have revealed a biphasic character with lifetimes of 135 μs and 870 μs at pH 4 [84]. A multiphasic kinetics for $P_{680}^{\bullet+}$ $Q_A^{\bullet-}$ recombination (with lifetimes of 170 μs, 800 μs and 6 ms) has been also observed in Tris-treated *Synechococcus* PS II core complexes under conditions where Y_Z was oxidized prior to the flash [22,85]. The kinetic characterization of $P_{680}^{\bullet+}Q_A^{\bullet-}$ recombination under physiological conditions is not straightforward and remains somewhat uncertain, due to the competing electron donation to $P_{680}^{\bullet+}$ from Y_Z. From other available kinetic data, obtained under conditions in which Y_Z is assumed to be oxidized by an appropriate pre-illumination regime [44,86,87] or in cyanobacterial PS II complexes from a Y_Z-deficient mutant, in which D1-Tyr161 had been replaced by a phenylalanine [60,62], different lifetimes, ranging from 80 μs to a few ms, have been estimated. It has to be mentioned that, in addition to the different conditions and systems in which measurements have been performed, $P_{680}^{\bullet+}Q_A^{\bullet-}$ kinetics reported in these studies are in general poorly resolved in the tens of μs time window after the laser flash.

Our attribution of both phase 3 and 4 to $P_{680}^{\bullet+}Q_A^{\bullet-}$ recombination, i.e. to the same electron transfer process, is further supported by the parallel response of their relative amplitudes to the incorporation of PS II into the trehalose glass and to matrix dehydration (Fig. 3B). The consistency of this interpretation appears even more clearly from Fig. 4, where the sum of the relative contributions of phase 1 and 2, ascribed to Y_Z oxidation, as well as the sum of the relative amplitudes of phase 3 and 4, interpreted as reflecting back electron transfer from $Q_A^{\bullet-}$, are plotted as a function of the residual water content of the matrix. The monotonic, smooth dependences obtained indicate that the relative contribution of electron donation from Y_Z, which accounts for ~90% of $P_{680}^{\bullet+}$ decay in the liquid phase (both in the absence and presence of a high trehalose concentration), decreases significantly upon transition to the glassy state (at ~9 water molecules per trehalose molecule), and is drastically reduced to 50% of the total when the content of residual water of the glassy matrix is decreased to about 4 water per trehalose molecules. Notably, further dehydration (at water contents between ~4 and ~1 water per trehalose molecule) does not further reduce the contribution of Y_Z oxidation to $P_{680}^{\bullet+}$ re-reduction after the flash. A similar response

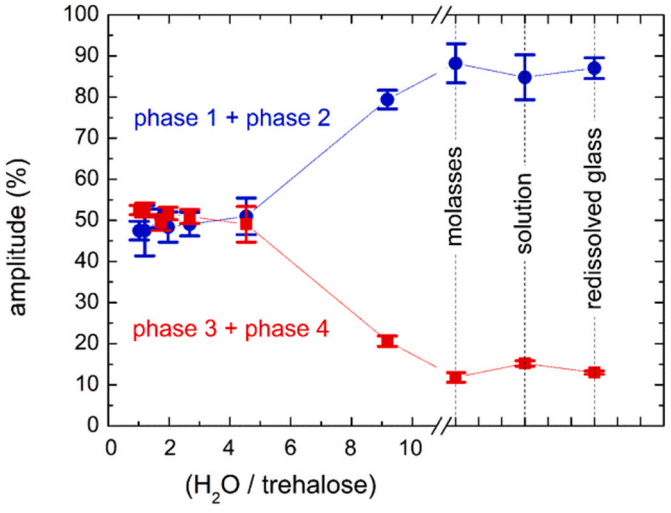

Fig. 4. Relative contribution to the kinetics of $P_{680}^{\bullet+}$ re-reduction of the sum of the two fastest (phase 1 and 2) and slowest (phase 3 and 4) kinetic components, obtained from the data of Fig. 3B.

to dehydration is found for the lifetimes of phase 1 and 2, which increase upon decreasing the hydration of the system down to about 4 water molecules per trehalose, but do not vary significantly at lower water contents (Fig. 3A).

Our kinetic analysis shows therefore that, upon incorporation of PS II into a progressively dehydrated trehalose glassy matrix, the electron transfer from Y_Z to $P_{680}^{\bullet+}$ is blocked in a progressively increasing fraction of the PS II population, which accounts for up to 50% of the total, when the residual water content of the matrix is decreased to about 4 water per trehalose molecule. In this PS II subpopulation $P_{680}^{\bullet+}$ re-reduction occurs by recombination of the charge pair $P_{680}^{\bullet+}Q_A^{\bullet-}$ (kinetic phase 3 and 4). Dehydration of the trehalose matrix slows down both electron transfer processes, Y_Z oxidation and $P_{680}^{\bullet+}Q_A^{\bullet-}$ recombination, the latter being retarded to a larger extent.

4. Discussion

4.1. Water bound to various photosynthetic reaction center complexes in trehalose-matrices

Water sorption by trehalose-PS II matrices as a function of relative humidity exhibits a peculiar behaviour when compared to that of trehalose-PS I glasses (Table 1). For all values of relative humidity tested, in trehalose matrices incorporating Mn-depleted or intact PS II complexes, a systematically larger water/trehalose molar ratio has been found. The difference is larger at low relative humidity, *r*. In fact, the hydration of trehalose-PS I matrices decreases monotonically upon decreasing the relative humidity down to $r = 11\%$; at variance, in trehalose-PS II matrices, the water/trehalose ratio decreases down to $r = 33\%$, but remains pretty constant at lower relative humidity, down to $r = 6\%$, indicating the presence of water molecules (approximately 1.1 per trehalose molecule in Mn-depleted PS II matrices) that are not removed even under extreme drought. Under these dry conditions ($r \leq 11\%$), both in trehalose-PS I complexes [19] and in trehalose glasses incorporating bRCs [14,88] at high trehalose/protein ratio ($\geq 5 \cdot 10^3$), a water/trehalose ratio ~0.5 has been determined, which coincides with the value measured in a pure trehalose matrix (in the absence of any incorporated protein) at the same relative humidity ($r = 11\%$) [78]. This finding shows that the number of residual water molecules bound to the embedded protein complexes is negligible when compared with the overall number of water adsorbed to the trehalose matrix, as expected for high trehalose/protein ratios. Although the trehalose-PS II matrices examined in the present study are characterized by comparably larger trehalose/PS II molar ratios ($>10^4$), two times larger water/trehalose ratios have been determined at $6\% \leq r \leq 33\%$, revealing an additional, large pool of tightly bound water molecules. We attribute this additional hydration of the matrix to water bound to the PS II complexes for the reasons outlined in the following.

Trehalose matrices embedding the Mn-depleted or the intact PS II complex are characterized by trehalose/PS II ratios of $4.8 \cdot 10^4$ and $3.5 \cdot 10^4$, respectively. These values, assuming molecular masses of 266 KDa and 350 KDa for the Mn-depleted and intact PS II complex, translate into trehalose/PS II mass ratios of 62 and 34, or into trehalose/PS II volume ratios of 33 and 21, respectively. Volume ratios have been estimated by assuming an average molecular volume of trehalose of $\sim 3.7 \cdot 10^2$ Å^3 [89] and volumes of $6.3 \cdot 10^5$ Å^3 and $5.4 \cdot 10^5$ Å^3 for the intact and Mn-depleted PS II complex (as obtained from the crystal structure of *Thermosynechococcus vulcanus* [90] by using the program Mol_Volume [91]). We expect, therefore, that a very large mass (and volume) of trehalose will surround each PS II complex embedded within the glassy matrix, and that the water adsorption properties of this bulk trehalose will negligibly be affected by the presence of the protein. The latter expectation is supported by a previous study, performed on trehalose-PS I matrices at comparably high sugar/protein ratios, in which, by analyzing W-band EPR spectra of nitroxide radical dispersed in the glass, we demonstrated that the incorporation of a large protein complex, as PS I, does not affect the distribution of residual water within the matrix [19]. Based on the above considerations, we infer that the additional hydration revealed by trehalose-PS II matrices, as compared to pure trehalose matrices, has to be ascribed to water molecules bound to the protein complex. The data of Table I indicate therefore that PS II binds a much larger number of water molecules as compared to PS I [19] and bRC [14,88]. This property, evidenced by the incorporation of PS II and PS I into the trehalose glassy matrix, appears to be qualitatively consistent with the crystallographic information available for the two complexes. Crystallographic structures of comparable resolution yield in fact a number of water molecules bound to the protein complex ranging from $2.6 \cdot 10^3$ to $4.0 \cdot 10^3$ for the PS II dimer [90,92,93] and between 300 and 900 for the PS I trimer [94–96]. Although several crystallographic water molecules found in the PS II complex are located in the protein interior or belong to channels or narrow clefts, the largest part of bound water molecules is located at the protein surface, mainly on the stromal and especially lumenal sides [90]. A quantitative estimate performed by using the UCSF Chimera program [77], based on the high-resolution structure determined by Umena and coworkers [90] (PDB ID: 3WU2), indicates that 82% of the total complement of the bound water (1554 per PS II monomer) lies on the protein surface and is exposed to the solvent (see Fig. S6 and its caption in Supplementary Material). This implies that the large majority of the excess water detected in trehalose-PS II complexes equilibrated at $r = 11\%$ has to be mainly ascribed to the protein hydration shell.

The water/trehalose ratio measured at low relative humidity in trehalose matrices incorporating intact PS II complexes is slightly larger than those of matrices embedding Mn-depleted PS II. This difference cannot however be attributed to a larger number of water molecules bound to the intact complex, as compared to the Mn-depleted PS II, because the trehalose/PS II ratio was about 30% smaller in the case of the matrix with the intact complex (see Table 1), and this difference increases per se the relative contribution of protein-bound water to the measured (average) water/trehalose ratio.

4.2. Implication for models of trehalose-matrix bioprotection

As discussed in the previous section, the PS II complex, embedded into an extensively dried trehalose matrix, retains a very large number of tightly bound water molecules, a substantial part of which belongs to the hydration shell coating the protein surface. This finding has important implications for understanding the structural and dynamic organization of trehalose-protein glasses as well as for clarifying the mechanism of trehalose bioprotection. The molecular mechanisms by which dehydrated trehalose glasses block the conformational dynamics of the embedded protein, leading to a dramatic structural stabilization of the protein under adverse environmental conditions (like high temperature and extreme drought), are still controversial. Different models have been proposed, some of which not mutually exclusive: (i) the *water replacement* hypothesis [97,98], assuming stabilization of the embedded protein via direct hydrogen bond formation between trehalose molecules of the matrix and surface groups of the proteins; (ii) the *high viscosity* hypothesis [99], postulating that the high viscosity of the glassy saccharide matrix plays the key role in preservation of the embedded protein by reducing the internal protein dynamics; (iii) the *water entrapment* hypothesis [100] proposing that residual water molecules are trapped at the protein-sugar interface, thus preserving its solvation and native structure within dehydrated glasses; (iv) the *anchorage* hypothesis [2,15,101], which combines features from model (ii) and (iii), postulating that the residual hydration shell of the incorporated protein forms multiple hydrogen bonds bridging surface amino-acid groups with sugar molecules in the matrix, while trehalose molecules makes very few direct hydrogen bonds contacts with the protein surface. According to the *anchorage* hypothesis, hydrogen bonds also connect trehalose molecules in the bulky matrix, which becomes progressively stiffened upon dehydration and, being dynamically coupled to the protein through its

hydration shell, locks the protein surface, hindering protein conformational dynamics.

The main difference between the proposed hypotheses summarized above is the fate of the protein hydration shell: models (iii) and (iv) assume that the glass-embedded protein retains its hydration shell within the matrix, while, according to the *water replacement* hypothesis (i), the water molecules of the hydration shell are replaced by bound sugar molecules. Our data, indicating that a very large number of water molecules remains bound at the surface of the PS II complex even within extensively dried trehalose matrices, disprove the *water replacement* model (i), strongly supporting the assumptions of the *water entrapment* (iii) and *anchorage* (iv) models.

4.3. Matrix effects on electron transfer

In the present study, we have focused on spinach Mn-depleted complexes. Treatment of PS II under alkaline conditions results in inactivation of oxygen evolving activity, dissociation of the extrinsic proteins of PS II, rapid Mn and Ca release and decrease in the efficiency of electron transfer from Q_A to the secondary quinone acceptor Q_B [84,102,103]. The lack of weakly bound Q_B in PS II preparations used in this work is likely due to treatment of membrane fragments with DM [64,104].

When interpreting the kinetics of $P_{680}^{\bullet+}$ re-reduction after a laser pulse in PS II preparations deprived of the WOC, it has to be considered that there are in principle several possible redox cofactors capable of donating electrons to $P_{680}^{\bullet+}$: (1) the tyrosine Y_Z, (2) the cytochrome b_{559}, (3) the tyrosine Y_D (Tyr-160 of the D2 subunit) and (4) the photoreduced quinone acceptor Q_A [61]. It should be stressed that transfer of an electron from Y_Z to $P_{680}^{\bullet+}$ is the dominant reaction [61], because electron donation from Y_Z occurs on a microsecond time scale, whereas cyt b_{559}, or Y_D reduce $P_{680}^{\bullet+}$ on a millisecond to second time scale in Mn-depleted PS II complexes [59,61,105,106]. Note that the photooxidation of both cyt b_{559} [61,107] and Y_D [106] has been observed under non physiological conditions (reviewed in [108] and [109]). Under the conditions of our measurements of $P_{680}^{\bullet+}$ reduction kinetics we can however exclude a contribution due to electron transfer from cyt b_{559}. In fact we did not observe any difference between $P_{680}^{\bullet+}$ signals recorded in dark adapted samples after a single flash and following a train of photoexcitation pulses fired at 2 Hz repetition rate (see Supplementary Material, Fig. S5). Since no exogenous electron donor was present, even in case of a low yield cyt b_{559} oxidation, we would have expected, following multiple-flash excitation, a progressive accumulation of the long lived state $Y_ZP_{680}Q_A^{\bullet-}$, resulting in a progressive decrease of the amplitude of photoxidized $P_{680}^{\bullet+}$, which was not detected. We conclude that, under our experimental conditions, the quantum yield of both oxidation of cyt b_{559}, and Y_D by $P_{680}^{\bullet+}$ is negligible in comparison to the quantum yield for formation of $Y_Z^{\bullet}$ per reaction center turnover. Thus, the first stable ion-radical pair state, which can be detected in our Mn-depleted complex is $Y_Z^{\bullet}Q_A^{\bullet-}$.

As described in detail in the Results section, different alternative approaches have been sounded out in analyzing the multiphasic kinetics of $P_{680}^{\bullet+}$ decay after a laser pulse, in terms of the sum of discrete exponential decay phases or of a continuous distribution of lifetimes (see also Supplementary Material, Figs. S3, S4 and Tables S1, S2, S3). The results obtained by using the MemExp software package, which combines non-linear least square minimization and the maximum entropy method, led us to conclude that the sum of four exponential decays provide the optimal description of the kinetics under all the conditions examined, i.e. in solution and in trehalose glassy matrices at different contents of residual water.

We have associated the two fastest kinetic components (phase 1 and phase 2 in Table 2 and Fig. 3), decaying on the μs time range, with the same electron transfer process, i.e. Y_Z oxidation by $P_{680}^{\bullet+}$, based on lifetime values and on the parallel response of the corresponding phase amplitudes to dehydration of the trehalose-PS II matrix (Fig. 3). Such a biphasic kinetics of Y_Z oxidation by $P_{680}^{\bullet+}$ in Mn-depleted PS II core particles has been reported by Junge and coworkers [84]. This study has provided evidence that biphasicity of Y_Z oxidation is related to its protonation state, the slower and faster component of Y_Z oxidation by $P_{680}^{\bullet+}$ (phases 2 and 1 of our kinetic analysis) reflecting electron transfer limited or not-limited, respectively, by proton transfer.

As already argued in the Results section, we have ascribed phases 3 and 4 of $P_{680}^{\bullet+}$ reduction kinetics to recombination of the charged $P_{680}^{\bullet+}Q_A^{\bullet-}$ pair in view of the lifetimes observed in liquid samples (solution, redissolved glass, trehalose molasses), which compare well with the range of lifetime values reported in previous studies, using different approaches (pre-oxidation of Y_Z or mutations of D1-Tyr161) to observe $P_{680}^{\bullet+}Q_A^{\bullet-}$ recombination [22,44,60,62,84–87]. Again, the attribution of phases 3 and 4 to a unique electron transfer process is in line with the parallel response of the amplitude of these phases to dehydration of the trehalose-PS II glassy matrix. Multiexponential kinetics of $P_{680}^{\bullet+}Q_A^{\bullet-}$ recombination have been previously reported [22,85], and attributed to different PS II conformational states, which do not interconvert on the time scale of charge recombination.

In solution, both in the absence or presence of trehalose, the two fastest phases, in the μs time range, dominate the re-reduction of $P_{680}^{\bullet+}$, accounting together for about 85% of the total decay. The addition of trehalose at high concentration (1.12 M) significantly slows down Y_Z oxidation, as shown by the almost doubled lifetime of phase 1 and 2 of $P_{680}^{\bullet+}$ reduction (Table 2). Such an effect appears to be related to the increased viscosity of the solution (by more than one order-of-magnitude [89,110,111]), suggesting that the protein dynamics involved in Y_Z oxidation is slaved to solvent motions. A similar, but more pronounced, effect is observed for $P_{680}^{\bullet+}Q_A^{\bullet-}$ recombination kinetics, since the lifetime of phase 3 and of phase 4 increase by a factor of 2 and approximately 4, respectively, in the presence of 1.12 M trehalose (Table 2). Interestingly, this behaviour resembles that observed for the kinetics of charge recombination from the primary charge separated state $P^{\bullet+}Q_A^{\bullet-}$ in bRCs of *Blastochloris* (*Bl*) *viridis*, previously named *Rhodopseudomonas viridis* [112]. In this bRC, the lifetime of $P^{\bullet+}Q_A^{\bullet-}$ recombination has been found to similarly increase upon increasing the solvent viscosity, modified by the addition of glycerol, sucrose or ethylene glycol; in this system, the viscosity dependence fitted a modified Kramers' equation [113], suggesting a viscosity induced damping of bRC protein vibrational modes coupled to electron transfer.

In the trehalose-PS II amorphous matrix characterized by a very high water content (≅ 10 water molecules per trehalose molecule), close to undergo transition from a glassy to a rubbery state, the lifetimes of all kinetic phases further increase to a limited extent, and do not change significantly when the content of residual water is reduced below about 4 water molecules per trehalose molecule. However, over the hydration range between ~10 and ~4 waters per trehalose molecule the major kinetic effect is observed, consisting in a large increase of the relative amplitudes of phase 3 and 4 at the expenses of phase 1 and 2. We conclude therefore that the contribution of Y_Z oxidation to $P_{680}^{\bullet+}$ re-reduction is drastically decreased from approximately 90% to 50%, and the relative contribution of $P^{\bullet+}Q_A^{\bullet-}$ recombination increases correspondingly (see Fig. 4).

Under physiological conditions, the study of $P^{\bullet+}Q_A^{\bullet-}$ recombination is hampered by the competition with forward electron transfer reactions rapidly re-reducing $P^{\bullet+}$. Our data show that the incorporation of PS II into trehalose matrices represents a new strategy to monitor $P^{\bullet+}Q_A^{\bullet-}$ recombination under relatively hydrated conditions. Such an approach can be of particular interest, when considering that $P^{\bullet+}Q_A^{\bullet-}$ recombination plays an important role in both photodamage and photoprotection of PS II [114].

Since over the hydration range between ~10 and ~4 water per trehalose molecule the lifetimes of the two phases related to Y_Z oxidation do not change significantly, the observed, progressive decrease in the contribution of Y_Z oxidation appears to reflect an *inhomogeneous* inhibition of this process, whereby, upon decreasing the matrix

hydration, Y_Z oxidation is blocked or dramatically slowed down, in a progressively increasing fraction of the PS II population. In this sub-population the drastically hampered Y_Z oxidation cannot compete kinetically with $P^{\bullet+}Q_A^{\bullet-}$ recombination.

We exclude the possibility that the decrease of phases 1 and 2 of $P_{680}^{\bullet+}$ re-reduction kinetics upon dehydration of the matrix is trivially due to pre-oxidation of Y_Z in the dark. This occurrence is extremely unlikely when considering that: (a) as shown in trehalose-bRC matrices [10], in dried multilayers of membrane fragments from photosynthetic bacteria [115], and in dehydrated films of PS II membrane fragments [63], sample dehydration results in a reducing redox ambient; (b) dehydration of trehalose-PS I glasses [19] did not result in dark pre-oxidation of P_{700}, a redox center with a midpoint potential of 450 mV, which is much lower than that of the ($Y_Z^{\bullet}/Y_Z$) pair, close to 1 V [35].

4.4. Mechanism of matrix-induced inhibition of electron transfer from Y_Z to $P_{680}^{\bullet+}$

The progressive block of Y_Z oxidation, observed at room temperature in trehalose matrices upon decreasing the residual water content, mimics the progressive block detected in hydrated, intact PS II complexes in the presence of glycerol, upon decreasing the temperature between 300 K and 200 K [23]. Noteworthy, such a parallel behaviour is shared by forward electron transfer processes catalyzed by other photosynthetic RCs, i.e. the Q_A^--to-Q_B electron transfer in bRC from *Rba. sphaeroides* [10,16,116], and electron transfer from F_X^- to the terminal F_A/F_B acceptors and from the photoreduced phylloquinones $A_1^{\bullet-}$ to the iron-sulfur centers in PS I complexes [19–21]. In order to explain the progressively reduced yield of Y_Z oxidation upon freezing at cryogenic temperatures, two alternatives have been considered in [23]: (a) an *heterogeneous* inhibition of the electron transfer reaction due to the trapping of the PS II complex into frozen conformational substates; (b) an *homogeneous* inhibition originating in the temperature dependence of the free energy change ΔG^0 for electron transfer, resulting in a decreasing driving force for Y_Z oxidation over the temperature range between 300 K and 100 K. The latter option is favoured by Schlodder and coworkers [23], based on the analysis of $P_{680}^{\bullet+}$ decay following multi-flash photoexcitation.

The increasing inhibition of Y_Z oxidation observed by us upon dehydration of the trehalose matrix at room temperature can equally be explained by an unfavorable free energy change for electron transfer, which could arise from the freezing of nuclear coordinates associated with *non-adiabatic* medium reorganization [117]. In the case of the room temperature dehydrated trehalose-PS II glassy matrix, such a freezing will originate from the dramatic hindering of protein dynamics, which has been shown to be drastically reduced upon dehydration of the trehalose-protein glass, due to the tight dynamical coupling between the embedded protein and the increasingly stiffened sugar matrix [2–4,14,88]. However, at variance with the proposed *homogenous* low temperature inhibition of Y_Z oxidation [23], the room temperature hindrance of PS II conformational dynamics in progressively dehydrated trehalose glasses implies an *heterogeneous* inhibition of electron transfer, i.e. the trapping of an increasing fraction of the PS II population in completely inactive conformation(s).

Hindering of PS II protein dynamics can cause inhibition of Y_Z oxidation through other mechanisms, including, besides the above mentioned block of specific, *non-adiabatic* reorganization modes, the inhibition of *adiabatic* protein relaxations resulting in energetic destabilization of the oxidized form of Y_Z and/or the increase of activation barriers preventing forward electron transfer to $P_{680}^{\bullet+}$. Since it is believed, based on the observed H/D isotope exchange effect, that in Mn-depleted PS II complexes proton transfer is involved in the rate-limiting step of Y_Z oxidation [62,84,118,119], it can be proposed that dehydration of the embedding trehalose matrix, critically increases the energy barrier to proton transfer. In fact, the structural and dynamical modifications of the protein hydration shell, caused by incorporation of Mn-depleted complexes into the dehydrated trehalose matrix, are likely to perturb the geometry of the hydrogen-bond network in the immediate Y_Z environment, which has become more hydrophilic due to the removal of the oxygen-evolving Mn cluster.

Whatever the detailed mechanism, our data indicate unequivocally that PS II conformational dynamics play a critical role in promoting forward electron transfer from Y_Z to $P_{680}^{\bullet+}$, as found for other forward electron transfer steps within PS I [19] and bRC [10].

In relation with the direct involvement of Y_Z (D1-Tyr161) dynamics in its oxidation by $P_{680}^{\bullet+}$, it may be relevant to consider the results of a time-resolved Laue diffraction study [120], aimed to identify light-induced structural changes in the bRC of *Bl. viridis*. Wohri and coworkers [120] have found that the largest conformational change observed over the whole structure of the complex following a short (3 ms) illumination, is localized to TyrL162, which corresponds to D1-Tyr161 in PS II. In the photoactivated conformation, the hydroxyl oxygen of TyrL162 has moved by 1.3 Å towards the photoxidized primary electron donor, the bacteriochlorophyll special pair P_{960}^+. Molecular dynamics simulations indicate that the photooxidation of P_{960} to P_{960}^+ changes the electrostatic environment of TyrL162, favoring its deprotonation; additionally, the deprotonated TyrL162 undergoes a conformational change reducing by ~1 Å its distance from P_{960}^+. Noteworthy, re-reduction of P_{960}^+ by heme c_{559} of the bound tetraheme cytochrome *c* subunit is inhibited at cryogenic temperatures, and mutation of TyrL162 affects the extent and temperature dependence of electron transfer inhibition [121]. The direct observation of TyrL162 re-orientation in response to photooxidation of P_{960} supports the suggestion [122,123] that the structural rearrangement and deprotonation of TyrL162, besides stabilizing primary charge separation, play an important role in the mechanism of electron transfer to P_{960}^+. Interestingly, the location of TyrL162 of *Bl. viridis* (between heme c_{559} and P_{960}) is functionally analogous to that of D1-Tyr161 (Y_Z) of PS II (between the WOC and P_{680}) (see Fig. 4 of ref. [120]). It is tempting to speculate that in the PS II complex, following P_{680} photooxidation, D1-Tyr161 undergoes a reorientation similar to that observed by Wohri and coworkers [120] for TyrL162 in the bRC from *Bl. viridis*, and that such a movement, bringing Y_Z closer to $P_{680}^{\bullet+}$, could govern Y_Z oxidation.

5. Conclusions

Desiccation of PS II in trehalose glassy matrices leads to the confinement of the protein internal mobility, which results in: (a) slowing of both forward (Y_Z oxidation) and backward (recombination between $Q_A^{\bullet-}$ and $P_{680}^{\bullet+}$) electron transfer; (b) *heterogeneous* inhibition of Y_Z oxidation in about half of the PS II population in which $P_{680}^{\bullet+}Q_A^{\bullet-}$ recombination takes place. The retardation of protein dynamics coupled to electron transfer in trehalose glasses is common to all three types of photosynthetic reaction center complexes, namely PS II, PS I and bRC. However, the maximal trehalose matrix effect in the case of PS II is observed at higher water/trehalose molar ratios as compared to PS I and bRC. This is consistent with the crystallographic data, which show a larger number of water molecules in PS II in contrast to PS I and bRC. The detection of a large pool of water molecules bound to PS II complexes embedded into extensively dehydrated trehalose matrices provides new insights into the structural and dynamic organization of trehalose-protein glassy matrices and into the mechanism of trehalose biopreservation, falsifying the *water replacement* hypothesis, while strongly supporting the *water entrapment* and *anchorage* models.

Declaration of competing interest

The authors declare that they have no known competing financial interests or personal relationships that could have appeared to influence the work reported in this paper.

Acknowledgements

This work was supported by grant from Russian Science Foundation (grant numbers 21-14-00229, 17-00-00201, 17-00-00218) to A.Yu.S., M.D.M., G.E.M. and L.A.V. Financial support from MIUR of Italy (RFO2018) is gratefully acknowledged by F. F., M.M. and G.V. A.Yu.S and M.D.M. acknowledge partial support from Lomonosov Moscow State University Program of Development. Molecular graphics and analyses have been performed with UCSF Chimera, developed by the Resource for Biocomputing, Visualization, and Informatics at the University of California, San Francisco, with support from NIH P41-GM103311.

Appendix A. Supplementary data

Supplementary data to this article can be found online at https://doi.org/10.1016/j.bbabio.2021.148413.

References

[1] J.L. Green, C.A. Angell, Phase relations and vitrification in saccharide water solutions and the trehalose anomaly, J. Phys. Chem. 93 (1989) 2880–2882.
[2] L. Cordone, G. Cottone, S. Giuffrida, G. Palazzo, G. Venturoli, C. Viappiani, Internal dynamics and protein-matrix coupling in trehalose-coated proteins, Biochim. Biophys. Acta, Proteins Proteomics 1749 (2005) 252–281.
[3] L. Cordone, G. Cottone, A. Cupane, A. Emanuele, S. Giuffrida, M. Levantino, Proteins in saccharides matrices and the trehalose peculiarity: biochemical and biophysical properties, Curr. Org. Chem. 19 (2015) 1684–1706.
[4] G. Cottone, S. Giuffrida, S. Bettati, S. Bruno, B. Campanini, M. Marchetti, S. Abbruzzetti, C. Viappiani, A. Cupane, A. Mozzarelli, L. Ronda, More than a confinement: "soft" and "hard" enzyme entrapment modulates biological catalyst function, Catalysts 9 (2019) 1024.
[5] M.T. Cicerone, M.J. Pikal, K.K. Qian, Stabilization of proteins in solid form, Adv. Drug Deliv. Rev. 93 (2015) 14–24.
[6] G. Bellavia, S. Giuffrida, G. Cottone, A. Cupane, L. Cordone, Protein thermal denaturation and matrix glass transition in different protein-trehalose-water systems, J. Phys. Chem. B 115 (2011) 6340–6346.
[7] L.M. Crowe, Lessons from nature: the role of sugars in anhydrobiosis, Comp. Biochem. Physiol. A 131 (2002) 505–513.
[8] C. Selva, M. Malferrari, R. Ballardini, A. Ventola, F. Francia, G. Venturoli, Trehalose preserves the integrity of lyophilized phycoerythrin-antihuman CD8 antibody conjugates and enhances their thermal stability in flow cytometric assays, J. Pharm. Sci. 102 (2013) 649–659.
[9] G. Palazzo, A. Mallardi, A. Hochkoeppler, L. Cordone, G. Venturoli, Electron transfer kinetics in photosynthetic reaction centers embedded in trehalose glasses: trapping of conformational substates at room temperature, Biophys. J. 82 (2002) 558–568.
[10] F. Francia, G. Palazzo, A. Mallardi, L. Cordone, G. Venturoli, Residual water modulates Q_A^--to-Q_B electron transfer in bacterial reaction centers embedded in trehalose amorphous matrices, Biophys. J. 85 (2003) 2760–2775.
[11] F. Francia, G. Palazzo, A. Mallardi, L. Cordone, G. Venturoli, Probing light-induced conformational transitions in bacterial photosynthetic reaction centers embedded in trehalose-water amorphous matrices, Biochim. Biophys. Acta Bioenerg. 1658 (2004) 50–57.
[12] A. Savitsky, M. Malferrari, F. Francia, G. Venturoli, K. Möbius, Bacterial photosynthetic reaction centers in trehalose glasses: coupling between protein conformational dynamics and electron-transfer kinetics as studied by laser-flash and high-field EPR spectroscopies, J. Phys. Chem. B 114 (2010) 12729–12743.
[13] F. Francia, M. Malferrari, S. Sacquin-Mora, G. Venturoli, Charge recombination kinetics and protein dynamics in wild type and carotenoid-less bacterial reaction centers: studies in trehalose glasses, J. Phys. Chem. B 113 (2009) 10389–10398.
[14] M. Malferrari, F. Francia, G. Venturoli, Retardation of protein dynamics by trehalose in dehydrated systems of photosynthetic reaction centers. Insights from electron transfer and thermal denaturation kinetics, J. Phys. Chem. B 119 (2015) 13600–13618.
[15] F. Francia, M. Dezi, A. Mallardi, G. Palazzo, L. Cordone, G. Venturoli, Protein-matrix coupling/uncoupling in "dry" systems of photosynthetic reaction center embedded in trehalose/sucrose: the origin of trehalose peculiarity, J. Am. Chem. Soc. 130 (2008) 10240–10246.
[16] D. Kleinfeld, M.Y. Okamura, G. Feher, Electron-transfer kinetics in photosynthetic reaction centers cooled to cryogenic temperatures in the charge-separated state: evidence for light-induced structural changes, Biochemistry 23 (1984) 5780–5786.
[17] M.S. Graige, G. Feher, M.Y. Okamura, Conformational gating of the electron transfer reaction $Q_A^-Q_B \rightarrow Q_AQ_B^-$ in bacterial reaction centers of *Rhodobacter sphaeroides* determined by a driving force assay, Proc. Natl. Acad. Sci. U. S. A. 95 (1998) 11679–11684.
[18] B.H. McMahon, J.D. Muller, C.A. Wraight, G.U. Nienhaus, Electron transfer and protein dynamics in the photosynthetic reaction center, Biophys. J. 74 (1998) 2567–2587.
[19] M. Malferrari, A. Savitsky, M.D. Mamedov, G.E. Milanovsky, W. Lubitz, K. Mobius, A.Y. Semenov, G. Venturoli, Trehalose matrix effects on charge-recombination kinetics in Photosystem I of oxygenic photosynthesis at different dehydration levels, Biochim. Biophys. Acta Bioenerg. 1857 (2016) 1440–1454.
[20] V. Kurashov, M. Gorka, G.E. Milanovsky, T.W. Johnson, D.A. Cherepanov, A. Y. Semenov, J.H. Golbeck, Critical evaluation of electron transfer kinetics in P_{700}-F_A/F_B, P_{700}-F_X, and P_{700}-A_1 Photosystem I core complexes in liquid and in trehalose glass, Biochim. Biophys. Acta Bioenerg. 1859 (2018) 1288–1301.
[21] G. Milanovsky, O. Gopta, A. Petrova, M. Mamedov, M. Gorka, D. Cherepanov, J. H. Golbeck, A. Semenov, Multiple pathways of charge recombination revealed by the temperature dependence of electron transfer kinetics in cyanobacterial photosystem I, Biochim. Biophys. Acta Bioenerg. 1860 (2019) 601–610.
[22] B. Hillmann, E. Schlodder, Electron transfer reactions in Photosystem II core complexes from *Synechococcus* at low temeprature - difference spectrum of $P680^+Q_A^-P680Q_A$ at 77 K, Biochim. Biophys. Acta Bioenerg. 1231 (1995) 76–88.
[23] E. Schlodder, M. Cetin, F. Lendzian, Temperature dependence of the oxidation kinetics of Tyr_Z and Tyr_D in oxygen-evolving photosystem II complexes throughout the range from 320 K to 5 K, Biochim. Biophys. Acta Bioenerg., 1847 (2015) 1283–1296.
[24] X. Tang, K. Satoh, The oxygen-evolving photosystem II core complex, FEBS Lett. 179 (1985) 60–64.
[25] M.M. Najafpour, G. Renger, M. Holynska, A.N. Moghaddam, E.M. Aro, R. Carpentier, H. Nishihara, J.J. Eaton-Rye, J.R. Shen, S.I. Allakhverdiev, Manganese compounds as water-oxidizing catalysts: from the natural water-oxidizing complex to nanosized manganese oxide structures, Chem. Rev. 116 (2016) 2886–2936.
[26] J.F. Allen, W.B.M. de Paula, S. Puthiyaveetil, J. Nield, A structural phylogenetic map for chloroplast photosynthesis, Trends Plant Sci. 16 (2011) 645–655.
[27] A. Williamson, B. Conlan, W. Hillier, T. Wydrzynski, The evolution of Photosystem II: insights into the past and future, Photosynth. Res. 107 (2011) 71–86.
[28] V.P. Shinkarev, C.A. Wraight, Oxygen evolution in photosynthesis: from unicycle to bicycle, Proc. Natl. Acad. Sci. U. S. A. 90 (1993) 1834–1838.
[29] F. Müh, C. Glockner, J. Hellmich, A. Zouni, Light-induced quinone reduction in photosystem II, Biochim. Biophys. Acta Bioenerg., 1817 (2012) 44–65.
[30] K. Ifuku, Localization and functional characterization of the extrinsic subunits of photosystem II: an update, Biosci. Biotechnol. Biochem. 79 (2015) 1223–1231.
[31] J.L. Roose, L.K. Frankel, M.P. Mummadisetti, T.M. Bricker, The extrinsic proteins of photosystem II: update, Planta 243 (2016) 889–908.
[32] F. Müh, A. Zouni, Structural basis of light-harvesting in the photosystem II core complex, Protein Sci. 29 (2020) 1090–1119.
[33] M. Karge, K.D. Irrgang, S. Sellin, R. Feinaugle, B. Liu, H.J. Eckert, H.J. Eichler, G. Renger, Effects of hydrogen deuterium exchange on photosynthetic water cleavage in PS II core complexes from spinach, FEBS Lett. 378 (1996) 140–144.
[34] C. Berthomieu, R. Hienerwadel, A. Boussac, J. Breton, B.A. Diner, Hydrogen bonding of redox-active tyrosine Z of photosystem II probed by FTIR difference spectroscopy, Biochemistry 37 (1998) 10547–10554.
[35] C. Tommos, G.T. Babcock, Proton and hydrogen currents in photosynthetic water oxidation, Biochim. Biophys. Acta Bioenerg. 1458 (2000) 199–219.
[36] K. Saito, J.R. Shen, T. Ishida, H. Ishikita, Short hydrogen bond between redox-active tyrosine Y_z and D1-His190 in the photosystem II crystal structure, Biochemistry 50 (2011) 9836–9844.
[37] W. Lubitz, M. Chrysina, N. Cox, Water oxidation in photosystem II, Photosynth. Res. 142 (2019) 105–125.
[38] F. Rappaport, B.A. Diner, Primary photochemistry and energetics leading to the oxidation of the (Mn)4Ca cluster and to the evolution of molecular oxygen in Photosystem II, Coord. Chem. Rev. 252 (2008) 259–272.
[39] F. Müh, A. Zouni, Light-induced water oxidation in photosystem II, Front. Biosci. 16 (2011) 3072–3132.
[40] D.J. Vinyard, G.W. Brudvig, Progress toward a molecular mechanism of water oxidation in photosystem II, in: M.A. Johnson, T.J. Martinez (Eds.), Annu. Rev. Phys. Chem. Vol 68, 2017, pp. 101–116.
[41] N. Cox, D.A. Pantazis, W. Lubitz, Current understanding of the mechanism of water oxidation in photosystem II and its relation to XFEL data, Annu. Rev. Biochem. 89 (2020) 795–820.
[42] D. Shevela, J. Messinger, Probing the turnover efficiency of photosystem II membrane fragments with different electron acceptors, Biochim. Biophys. Acta Bioenerg., 1817 (2012) 1208–1212.
[43] D. Shevela, G. Ananyev, A.K. Vatland, J. Arnold, F. Mamedov, L.A. Eichacker, G. C. Dismukes, J. Messinger, 'Birth defects' of photosystem II make it highly susceptible to photodamage during chloroplast biogenesis, Physiol. Plant. 166 (2019) 165–180.
[44] H. Conjeaud, P. Mathis, The effect of pH on the reduction kinetics of P-680 in tris-treated chloroplasts, Biochim. Biophys. Acta Bioenerg. 590 (1980) 353–359.
[45] E. Schlodder, B. Meyer, pH dependence of oxygen evolution and reduction kinetics of photooxidized chlorophyll a_{II} (P-680) in Photosystem II particles from *Synechococcus* sp, Biochim. Biophys. Acta 890 (1987) 23–31.
[46] A.M.A. Hays, I.R. Vassiliev, J.H. Golbeck, R.J. Debus, Role of D1-His190 in the proton-coupled oxidation of tyrosine Y_Z in manganese-depleted photosystem II, Biochemistry 38 (1999) 11851–11865.
[47] M.J. Schilstra, F. Rappaport, J.H.A. Nugent, C.J. Barnett, D.R. Klug, Proton/hydrogen transfer affects the S-state-dependent microsecond phases of $P680^+$ reduction during water splitting, Biochemistry 37 (1998) 3974–3981.
[48] F. Rappaport, J. Lavergne, Coupling of electron and proton transfer in the photosynthetic water oxidase, Biochim. Biophys. Acta Bioenerg., 1503 (2001) 246–259.

[49] S.K. Chamorovsky, D.A. Cherepanov, C.S. Chamorovsky, A.Y. Semenov, Correlation of electron transfer rate in photosynthetic reaction centers with intraprotein dielectric properties, Biochim. Biophys. Acta Bioenerg., 1767 (2007) 441–448.

[50] A. Krieger, A.W. Rutherford, G.N. Johnson, On the determination of redox midpoint potential of the primary quinone electron acceptor, Q_A, in Photosystem II, Biochim. Biophys. Acta-Bioenergetics, 1229 (1995) 193–201.

[51] G.N. Johnson, A.W. Rutherford, A. Krieger, A change in the midpoint potential of the quinone Q_A in photosystem II associated with photoactivation of oxygen evolution, Biochim. Biophys. Acta Bioenerg. 1229 (1995) 202–207.

[52] S.I. Allakhverdiev, T. Tsuchiya, K. Watabe, A. Kojima, D.A. Los, T. Tomo, V. V. Klimov, M. Mimuro, Redox potentials of primary electron acceptor quinone molecule (Q_A^-) and conserved energetics of photosystem II in cyanobacteria with chlorophyll a and chlorophyll d, Proc. Natl. Acad. Sci. U. S. A. 108 (2011) 8054–8058.

[53] Y. Kato, T. Noguchi, Long-range interaction between the Mn_4CaO_5 cluster and the non-heme iron center in photosystem II as revealed by FTIR spectroelectrochemistry, Biochemistry 53 (2014) 4914–4923.

[54] Y. Kato, R. Nagao, T. Noguchi, Redox potential of the terminal quinone electron acceptor Q_B in photosystem II reveals the mechanism of electron transfer regulation, Proc. Natl. Acad. Sci. U. S. A. 113 (2016) 620–625.

[55] M. Zhang, M. Bommer, R. Chatterjee, R. Hussein, J. Yano, H. Dau, J. Kern, H. Dobbek, A. Zouni, Structural insights into the light-driven auto-assembly process of the water oxidizing Mn4CaO5-cluster in photosystem II, Elife 6 (2017).

[56] Y. Kato, A. Ohira, R. Nagao, T. Noguchi, Does the water-oxidizing Mn_4CaO_5 cluster regulate the redox potential of the primary quinone electron acceptor Q_A in photosystem II? A study by Fourier transform infrared spectroelectrochemistry, Biochim. Biophys. Acta Bioenerg., 1860 (2019).

[57] R. de Wijn, H.J. van Gorkom, The rate of charge recombination in Photosystem II, Biochim. Biophys. Acta Bioenerg., 1553 (2002) 302–308.

[58] J. Haveman, P. Mathis, Flash-induced absorption changes of the primary donor of photosystem II at 820 nm in chloroplasts inhibited by low pH or tris-treatment, Biochim. Biophys. Acta Bioenerg. 440 (1976) 346–355.

[59] S. Reinman, P. Mathis, H. Conjeaud, A. Stewart, Kinetics of reduction of the primary donor of Photosystem II. Influence of pH in various preparations, Biochim. Biophys. Acta Bioenerg. 635 (1981) 429–433.

[60] J.G. Metz, P.J. Nixon, M. Rogner, G.W. Brudvig, B.A. Diner, Directed alteration of the D1 polypeptide of photosystem II: evidence that tyrosine-161 is the redox component, Z, connecting the oxygen-evolving complex to the primary electron donor, P680, Biochemistry 28 (1989) 6960–6969.

[61] C.A. Buser, L.K. Thompson, B.A. Diner, G.W. Brudvig, Electron-transfer reactions in manganese-depleted photosystem II, Biochemistry 29 (1990) 8977–8985.

[62] B.A. Diner, D.A. Force, D.W. Randall, R.D. Britt, Hydrogen bonding, solvent exchange, and coupled proton and electron transfer in the oxidation and reduction of redox-active tyrosine Yz in Mn-depleted core complexes of Photosystem II, Biochemistry 37 (1998) 17931–17943.

[63] O. Kaminskaya, G. Renger, V.A. Shuvalov, Effect of dehydration on light-induced reactions in photosystem II: photoreactions of cytochrome b559, Biochemistry 42 (2003) 8119–8132.

[64] E. Haag, K.D. Irrgang, E.J. Boekema, G. Renger, Functional and structural analysis of photosystem II core complexes from spinach with high oxygen evolution capacity, Eur. J. Biochem. 189 (1990) 47–53.

[65] R.J. Porra, W.A. Thompson, P.E. Kriedemann, Determination of accurate extinction coefficients and simultaneous equations for assaying chlorophyll *a* and chorophyll *b* extracted with 4 different solvents: verification of the concentration of chlorophyll standards by atomic absorption spectroscopy, Biochim. Biophys. Acta 975 (1989) 384–394.

[66] M. Malferrari, F. Francia, G. Venturoli, Coupling between electron transfer and protein-solvent dynamics: FTIR and laser-flash spectroscopy studies in photosynthetic reaction center films at different hydration levels, J. Phys. Chem. B 115 (2011) 14732–14750.

[67] M. Malferrari, G. Venturoli, F. Francia, A. Mezzetti, A new method for D2O/H2O exchange in infrared spectroscopy of proteins, Spectroscopy 27 (2012) 337–342.

[68] L. Greenspan, Humidity fixed points of binary saturated aqueous solutions, J. Res. Natl. Bur. Stand. A 814 (1977) 89–96.

[69] W.F. McClure, H. Maeda, J. Dong, Y.L. Liu, Y. Ozaki, Two-dimensional correlation of Fourier transform near-infrared and Fourier Transform Raman spectra I: mixtures of sugar and protein, Appl. Spectrosc. 50 (1996) 467–475.

[70] Y. Hattori, M. Otsuka, NIR spectroscopic study of the dissolution process in pharmaceutical tablets, Vib. Spectrosc. 57 (2011) 275–281.

[71] P. Mathis, P. Setif, Near infra-red absorption spectra of the chlorophyll a cations and triplet state *in vitro* and *in vivo*, Isr. J. Chem. 21 (1981) 316–320.

[72] S.W. Provencher, CONTIN: a general purpose constrained regularization program for inverting noisy linear algebraic and integral equations, Comput. Phys. Commun. 27 (1982) 229–242.

[73] P.J. Steinbach, R. Ionescu, C.R. Matthews, Analysis of kinetics using a hybrid maximum-entropy/nonlinear-least-squares method: application to protein folding, Biophys. J. 82 (2002) 2244–2255.

[74] P.J. Steinbach, Filtering artifacts from lifetime distributions when maximizing entropy using a bootstrapped model, Anal. Biochem. 427 (2012) 102–105.

[75] J.M. Beechem, Global analysis of biochemical and biophysical data, Methods Enzymol. 210 (1992) 37–54.

[76] A.R. Holzwarth, Data analysis of time-resolved measurements, in: J. Amesz, A. J. Hoff (Eds.), Biophysical Techniques in Photosynthesis. Advances in Photosynthesis and Respiration, Kluwer Academic Publishers, Dordrech, The Netherlands, 1996, pp. 75–92.

[77] E.F. Pettersen, T.D. Goddard, C.C. Huang, G.S. Couch, D.M. Greenblatt, E. C. Meng, T.E. Ferrin, U.C.S.F. Chimera, A visualization system for exploratory research and analysis, J. Comput. Chem. 25 (2004) 1605–1612.

[78] M. Malferrari, A. Nalepa, G. Venturoli, F. Francia, W. Lubitz, K. Möbius, A. Savitsky, Structural and dynamical characteristics of trehalose and sucrose matrices at different hydration levels as probed by FTIR and high-field EPR, Phys. Chem. Chem. Phys. 16 (2014) 9831–9848.

[79] S. Giuffrida, G. Cottone, F. Librizzi, L. Cordone, Coupling between the thermal evolution of the heme pocket and the external matrix structure in trehalose coated carboxymyoglobin, J. Phys. Chem. B 107 (2003) 13211–13217.

[80] P.J. Steinbach, K. Chu, H. Frauenfelder, J.B. Johnson, D.C. Lamb, G.U. Nienhaus, T.B. Sauke, R.D. Young, Determination of rate distributions from kinetic experiments, Biophys. J. 61 (1992) 235–245.

[81] D.L. Phillips, A technique for the numerical solution of certain integral equations of the first kind, J. Assoc. Comput. Mach. 9 (1962) 84–97.

[82] P.J. Steinbach, Inferring lifetime distributions from kinetics by maximizing entropy using a bootstrapped model, J. Chem. Inf. Comput. Sci. 42 (2002) 1476–1478.

[83] P.R. Bevington, Data Reduction and Error Analysis for the Physical Sciences, McGraw-Hill, New York, 1969.

[84] R. Ahlbrink, M. Haumann, D. Cherepanov, O. Bogershausen, A. Mulkidjanian, W. Junge, Function of tyrosine Z in water oxidation by photosystem II: electrostatical promotor instead of hydrogen abstractor, Biochemistry 37 (1998) 1131–1142.

[85] S. Gerken, J.P. Dekker, E. Schlodder, H.T. Witt, Studies on the multiphasic charge recombination between chlorophyll a_2^+ (P-680$^+$) and plastoquinone Q_A^- in photosystem II complexes. Ultraviolet difference spectrum of Chl-a_{II}^+/Chl-a_{II}, Biochim. Biophys. Acta 977 (1989) 52–61.

[86] H. Conjeaud, P. Mathis, G. Paillotin, Primary and secondary electron donors in Photosystem II of chloroplasts. Rates of electron transfer and location in the membrane, Biochim. Biophys. Acta Bioenerg. 546 (1979) 280–291.

[87] S. Reinman, P. Mathis, Influence of temperature on Photosystem II electron transfer reactions, Biochim. Biophys. Acta Bioenerg. 635 (1981) 249–258.

[88] M. Malferrari, A. Savitsky, W. Lubitz, K. Mobius, G. Venturoli, Protein immobilization capabilities of sucrose and trehalose glasses: the effect of protein/sugar concentration unraveled by high-field EPR, J. Phys. Chem. Lett. 7 (2016) 4871–4877.

[89] D.P. Miller, J.J. de Pablo, H. Corti, Thermophysical properties of trehalose and its concentrated aqueous solutions, Pharm. Res. 14 (1997) 578–590.

[90] Y. Umena, K. Kawakami, J.-R. Shen, N. Kamiya, Crystal structure of oxygen-evolving photosystem II at a resolution of 1.9Å, Nature 473 (2011) 55–60.

[91] A. Balaeff. https://www.ks.uiuc.edu/Development/MDTools/molvolume/.

[92] M. Suga, F. Akita, K. Hirata, G. Ueno, H. Murakami, Y. Nakajima, T. Shimizu, K. Yamashita, M. Yamamoto, H. Ago, J.-R. Shen, Native structure of photosystem II at 1.95 Å resolution viewed by femtosecond X-ray pulses, Nature 517 (2015) 99–103.

[93] M. Suga, F. Akita, K. Yamashita, Y. Nakajima, G. Ueno, H. Li, T. Yamane, K. Hirata, Y. Umena, S. Yonekura, L.-J. Yu, H. Murakami, T. Nomura, T. Kimura, M. Kubo, S. Baba, T. Kumasaka, K. Tono, M. Yabashi, H. Isobe, K. Yamaguchi, M. Yamamoto, H. Ago, J.-R. Shen, An oxyl/oxo mechanism for oxygen-oxygen coupling in PSII revealed by an x-ray free-electron laser, Science 366 (2019) 334–338.

[94] P. Jordan, P. Fromme, H.T. Witt, O. Klukas, W. Saenger, N. Krauß, Three-dimensional structure of cyanobacterial photosystem I at 2.5Å resolution, Nature 411 (2001) 909–917.

[95] K. Kato, T. Shinoda, R. Nagao, S. Akimoto, T. Suzuki, N. Dohmae, M. Chen, S. I. Allakhverdiev, J.-R. Shen, F. Akita, N. Miyazaki, T. Tomo, Structural basis for the adaptation and function of chlorophyll f in photosystem I, Nat. Commun. 11 (2020) 238.

[96] T. Malavath, I. Caspy, S.Y. Netzer-El, D. Klaiman, N. Nelson, Structure and function of wild-type and subunit-depleted photosystem I in *Synechocystis*, Biochim. Biophys. Acta Bioenerg., 1859 (2018) 645–654.

[97] J.F. Carpenter, J.H. Crowe, An infrared spectroscpopic study of the interactions of carbohydrates with dried proteins, Biochemistry 28 (1989) 3916–3922.

[98] S.D. Allison, B. Chang, T.W. Randolph, J.F. Carpenter, Hydrogen bonding between sugar and protein is responsible for inhibition of dehydration-induced protein unfolding, Arch. Biochem. Biophys. 365 (1999) 289–298.

[99] J.G. Sampedro, S. Uribe, Trehalose-enzyme interactions result in structure stabilization and activity inhibition. The role of viscosity, Mol. Cell. Biochem. 256 (2004) 319–327.

[100] P.S. Belton, A.M. Gil, IR and Raman spectroscopic studies of the interaction of trehalose with hen egg white lysozyme, Biopolymers 34 (1994) 957–961.

[101] A. Nalepa, M. Malferrari, W. Lubitz, G. Venturoli, K. Mobius, A. Savitsky, Local water sensing: water exchange in bacterial photosynthetic reaction centers embedded in a trehalose glass studied using multiresonance EPR, Phys. Chem. Chem. Phys. 19 (2017) 28388–28400.

[102] J. Cole, M. Boska, N.V. Blough, K. Sauer, Reversible and irreversible effects of alkaline pH on photosystem II electron-transfer reactions, Biochim. Biophys. Acta 848 (1986) 41–47.

[103] S.V. Baranov, A.M. Tyryshkin, D. Katz, G.C. Dismukes, G.M. Ananyev, V. V. Klimov, Bicarbonate is a native cofactor for assembly of the manganese cluster of the photosynthetic water oxidizing complex. Kinetics of reconstitution of O_2 evolution by photoactivation, Biochemistry 43 (2004) 2070–2079.

[104] H.M. Gleiter, E. Haag, Y. Inoue, G. Renger, Functional characterization of a purified homogeneous photosystem II core complex with high oxygen evolution capacity from spinach, Photosynth. Res. 35 (1993) 41–53.

[105] A. Boussac, A.L. Etienne, Oxido-reduction kinetics of signal II slow in tris-washed chloroplasts, Biochem. Biophys. Res. Commun. 109 (1982) 1200–1205.
[106] K. Saito, A.W. Rutherford, H. Ishikita, Mechanism of tyrosine D oxidation in Photosystem II, Proc. Natl. Acad. Sci. U. S. A. 110 (2013) 7690–7695.
[107] O.P. Kaminskaya, V.A. Shuvalov, Analysis of the transformation effect in cytochrome b559 of photosystem II in terms of the model of the heme-quinone redox interaction, Biochim. Biophys. Acta Bioenerg., 1859 (2018) 1161–1172.
[108] D.H. Stewart, G.W. Brudvig, Cytochrome b_{559} of photosystem II, Biochim. Biophys. Acta Bioenerg., 1367 (1998) 63–87.
[109] F. Müh, A. Zouni, Cytochrome b559 in photosystem II, in: W.A. Cramer, T. Kallas (Eds.), Cytochrome Complexes: Evolution, Structures, Energy Transduction, and Signaling, Advances in Photosynthesis and Respiration, Springer Science, 2016, pp. 143–175.
[110] M. Rampp, C. Buttersack, H.D. Ludemann, c,T-dependence of the viscosity and the self-diffusion coefficients in some aqueous carbohydrate solutions, Carbohydr. Res. 328 (2000) 561–572.
[111] G. Palazzo, F. Francia, A. Mallardi, M. Giustini, F. Lopez, G. Venturoli, Water activity regulates the Q_A^- to Q_B electron transfer in photosynthetic reaction centers from *Rhodobacter sphaeroides*, J. Am. Chem. Soc. 130 (2008) 9353–9363.
[112] R.J. Shopes, C.A. Wraight, Charge recombination from the $P^+Q_A^-$ state in reaction centers from *Rhodopseudomonas viridis*, Biochim. Biophys. Acta 893 (1987) 409–425.
[113] D. Beece, L. Eisenstein, H. Frauenfelder, D. Good, M.C. Marden, L. Reinisch, A. H. Reynolds, L.B. Sorensen, K.T. Yue, Solvent viscosity and protein dynamics, Biochemistry 19 (1980) 5147–5157.
[114] I. Vass, K. Cser, Janus-faced charge recombinations in photosystem II photoinhibition, Trends Plant Sci. 14 (2009) 200–205.
[115] C. Lieutaud, W. Nitschke, A. Vermeglio, P. Parot, B. Schoepp-Cothenet, HiPIP in Rubrivivax gelatinosus is firmly associated to the membrane in a conformation efficient for electron transfer towards the photosynthetic reaction centre, BBA-Bioenergetics, 1557 (2003) 83–90.
[116] Q. Xu, M.R. Gunner, Trapping conformational intermediate states in the reaction center protein from photosynthetic bacteria, Biochemistry 40 (2001) 3232–3241.
[117] K. Brettel, Electron transfer and arrangement of the redox cofactors in photosystem I, Biochim. Biophys. Acta Bioenerg., 1318 (1997) 322–373.
[118] A.M.A. Hays, I.R. Vassiliev, J.H. Golbeck, R.J. Debus, Role of D1-His190 in proton-coupled electron transfer reactions in photosystem II: a chemical complementation study, Biochemistry 37 (1998) 11352–11365.
[119] F. Rappaport, A. Boussac, D.A. Force, J. Peloquin, M. Brynda, M. Sugiura, S. Un, R.D. Britt, B.A. Diner, Probing the coupling between proton and electron transfer in photosystem II core complexes containing a 3-fluorotyrosine, J. Am. Chem. Soc. 131 (2009) 4425–4433.
[120] A.B. Wohri, G. Katona, L.C. Johansson, E. Fritz, E. Malmerberg, M. Andersson, J. Vincent, M. Eklund, M. Cammarata, M. Wulff, J. Davidsson, G. Groenhof, R. Neutze, Light-induced structural changes in a photosynthetic reaction center caught by Laue diffraction, Science 328 (2010) 630–633.
[121] J.M. Ortega, B. Dohse, D. Oesterhelt, P. Mathis, Low-temperature electron transfer from cytochrome to the special pair in *Rhodopseudomonas viridis*: role of the L162 residue, Biophys. J. 74 (1998) 1135–1148.
[122] B. Cartling, A mechanism of temperature dependent electron transfer reactions in biological systems, J. Chem. Phys. 95 (1991) 317–322.
[123] B. Cartling, An electron transfer switch in photosynthetic reaction centra, Chem. Phys. Lett. 196 (1992) 128–132.